

RESEARCH ARTICLE

Network supporting contextual fear learning after dorsal hippocampal damage has increased dependence on retrosplenial cortex

Cesar A. O. Coelho¹, Tatiana L. Ferreira², Juliana C. Kramer-Soares¹, João R. Sato², Maria Gabriela M. Oliveira^{1*}

1 Departamento de Psicobiologia, Universidade Federal de São Paulo - UNIFESP, São Paulo, São Paulo, Brazil, **2** Centro de Matemática, Computação e Cognição, Universidade Federal do ABC, UFABC, São Bernardo do Campo, São Paulo, Brazil

* gabriela.oliveira@unifesp.br



OPEN ACCESS

Citation: Coelho CAO, Ferreira TL, Kramer-Soares JC, Sato JR, Oliveira MGM (2018) Network supporting contextual fear learning after dorsal hippocampal damage has increased dependence on retrosplenial cortex. *PLoS Comput Biol* 14(8): e1006207. <https://doi.org/10.1371/journal.pcbi.1006207>

Editor: Daniel Bush, University College London, UNITED KINGDOM

Received: November 30, 2017

Accepted: May 15, 2018

Published: August 7, 2018

Copyright: © 2018 Coelho et al. This is an open access article distributed under the terms of the [Creative Commons Attribution License](https://creativecommons.org/licenses/by/4.0/), which permits unrestricted use, distribution, and reproduction in any medium, provided the original author and source are credited.

Data Availability Statement: All relevant data are within the paper and its Supporting Information files.

Funding: This work received funding from FAPESP #2010/16295-1 (<http://bv.fapesp.br/en/auxilios/29913/hippocampal-influence-on-the-expression-of-creb-pcreb-in-the-amygdala-nuclei-after-contextual-fear-c/>), FAPESP #2012/17619-0 (CAOC's PhD fellowship; <http://bv.fapesp.br/en/bolsas/139048/network-analysis-of-contextual->

Abstract

Hippocampal damage results in profound retrograde, but no anterograde amnesia in contextual fear conditioning (CFC). Although the content learned in the latter have been discussed, alternative regions supporting CFC learning were seldom proposed and never empirically addressed. Here, we employed network analysis of pCREB expression quantified from brain slices of rats with dorsal hippocampal lesion (dHPC) after undergoing CFC session. Using inter-regional correlations of pCREB-positive nuclei between brain regions, we modelled functional networks using different thresholds. The dHPC network showed small-world topology, equivalent to SHAM (control) network. However, diverging hubs were identified in each network. In a direct comparison, hubs in both networks showed consistently higher centrality values compared to the other network. Further, the distribution of correlation coefficients was different between the groups, with most significantly stronger correlation coefficients belonging to the SHAM network. These results suggest that dHPC network engaged in CFC learning is partially different, and engage alternative hubs. We next tested if pre-training lesions of dHPC and one of the new dHPC network hubs (perirhinal, Per; or disgranular retrosplenial, RSC, cortices) would impair CFC. Only dHPC-RSC, but not dHPC-Per, impaired CFC. Interestingly, only RSC showed a consistently higher centrality in the dHPC network, suggesting that the increased centrality reflects an increased functional dependence on RSC. Our results provide evidence that, without hippocampus, the RSC, an anatomically central region in the medial temporal lobe memory system might support CFC learning and memory.

Author summary

When determined cognitive performances are not affected by brain lesions of regions generally involved in that performance, the interpretation is that the remaining regions can promote function despite of (or compensate) the damaged one. In contextual fear conditioning, a memory model largely used in laboratory rodents, hippocampal lesions produce

[fear-conditioning-learning-in-the-absence-of-hippocampus/?q=2012/17619-0](#)), and FAPESP #2016/25755-2. The funders had no role in study design, data collection and analysis, decision to publish, or preparation of the manuscript.

Competing interests: The authors have declared that no competing interests exist.

amnesia for events occurred before, but not after the lesion, although the hippocampus is known to be important for new learning. Addressing how the brain can overcome lesion in animal models has always been challenging as it requires large-scale brain mapping. Here, we quantified 30 brain regions and used mathematical tools to model how a brain network can support contextual fear learning after hippocampal loss. We described that the damaged network preserved general interactivity characteristics, although different brain regions were identified as highly important for the network (e.g. highly connected). Further, we empirically validated our network model by performing double lesions of the hippocampus and the alternative hubs observed in the network models. We verified that double lesion of the hippocampus and retrosplenial cortex, one of the hubs, impaired contextual fear learning. We provide evidence that without hippocampus, the remaining network relies on alternative important regions from the memory system to coordinate contextual fear learning.

Introduction

Brain lesions provide evidence primarily about the extent to which a brain function can persevere in the absence of the damaged region. A preserved cognitive function or behavior after lesion is generally interpreted as alternative ‘brain routes’ being still able to meet the cognitive demands [1, 2]. In contextual fear conditioning (CFC), hippocampal lesions reveal a complex relation to contextual memory, as they result in profound retrograde amnesia (of pre-lesion events), but often result in no anterograde amnesia [post-lesion events; 3, 4, 5] under defined circumstances [6], suggesting that new learning can be supported by the reminiscent regions. Evidence for hippocampal participation in CFC acquisition have been provided by manipulations ranging from pharmacological injections such as muscarinic [7] and NMDA receptors blockade [8], to optogenetic approaches [9]. Thus, although hippocampus participates in CFC learning if it is functional during acquisition, CFC learning can occur after hippocampal loss.

The CFC learning after hippocampal lesion inspired cognitively-oriented hypotheses about the content learned by non-hippocampal regions. Although these accounts differ on whether the contextual representation without hippocampus is fragmented [elemental; 10, 11] or is—still—a configural representation [reviewed in 12], it is well accepted that learning under hippocampal loss is likely to be 1) different in terms of content learned, 2) less efficient and 3) more prone to generalization and decay over time [12–14]. It is also accepted that the hippocampus has preference over the non-hippocampal regions. This accounts for the impaired CFC observed after temporary manipulations, during which hippocampus inhibits the non-hippocampal regions while unable form long-term memory [12]. However, little attention has been given to the remaining regions supporting CFC learning. Although parahippocampal cortices were pointed out as putative candidates [11], the regions supporting CFC learning after hippocampal lesion have not been empirically addressed. Investigating how these regions learn and store CFC information can help to understand the dynamics of hippocampal function and its interactions within the memory systems.

There is evidence for a large number of regions to compose the neural circuits involved in CFC [15, 16] and spatial/contextual memory [17]. Understanding how a function/behavior can still be supported after lesion requires assessing complex interactions among the remaining regions and the changes in their engagement. Network approaches assess complex brain interactions based on the representation of elements (i.e. brain regions, neurons) and

connection concepts (i.e. projections, functional connectivity), and offer quantitative tools for a data-driven assessment of network characteristics related to brain structure and function [18].

Large-scale network studies based on structural and functional MRI data have been paving a solid ground in cognitive neuroscience [19, 20]. They have explored functional network topology in the brain [21] and its importance to learning [22] and emotion [23]. Network studies have also been useful in identifying crucial brain regions (hubs) for network function [24], and to identify functional network changes after traumatic brain injuries [25] and in psychiatric disorders [26, 27]. Some studies took advantage of rodent models and employed network analysis in the expression of the activity-dependent gene *c-fos* after remote CFC retrieval [28] and later empirically interrogated the network hubs given by the model [29]. Here, we used a similar rationale to investigate how the brain support CFC learning after hippocampal lesion. We used the phosphorylated cAMP response element binding (pCREB, active form of CREB), which is critical to learning-induced synaptic plasticity [30], as our marker of brain region engagement; and examined activation and co-activation of brain regions of hippocampectomized rats after a CFC session. Using network analysis, we examined how the post-lesion network might support CFC learning and memory. We hypothesized that different network attributes in the ‘damaged network’ could be underlying CFC learning after hippocampal lesion. Further, we performed double lesions to empirically validate group differences found in the network analysis. These double lesions tested whether the group differences revealed network changes supporting CFC learning after hippocampal loss (Fig 1).

Results

Experiment 1—Network underlying contextual fear learning in the absence of dHPC

Experiment 1 aimed to explore how CFC learning under dHPC damage changes other brain regions activity and interactivity compared to CFC learning in control rats. We compared pCREB expression levels between the groups in 30 brain regions (Fig 2) and modelled functional networks based on pCREB expression correlations. Then we employed network tools to explore differences between damaged and control groups. In Experiment 1, the rats initially underwent bilateral electrolytic lesions in the dHPC or SHAM surgery. After surgical recovery, the rats underwent a CFC training session. Half the cohort was perfused 3 h after the training session, and their brains processed for pCREB immunolabelling. CREB is a transcription factor involved in neuronal plasticity [30]. CREB is phosphorylated into pCREB after neuronal activity, which is taken in this study as a proxy of brain region engagement. The other half of the cohort was returned to the homecage and tested for contextual fear memory 48 h later. A group of immediate shock controls (Imm) was added to the cohort that was tested for contextual fear memory.

dHPC damage does not alter CFC memory

The histological examination of dHPC lesions revealed that the cellular loss was overall confined to the dorsal part of the hippocampus, with occasional lesion to the overlaying cortex due to the electrode insertion (Fig 3A). The cohort tested for contextual memory had the freezing behavior measured as memory index, and was compared among the groups. The sample size in the memory test cohort was 32 (SHAM: N = 12; dHPC: N = 12; Imm: N = 8). A bootstrapped one-way ANOVA showed a significant group effect ($F_{2,29} = 8.822$, $p = 0.0011$).

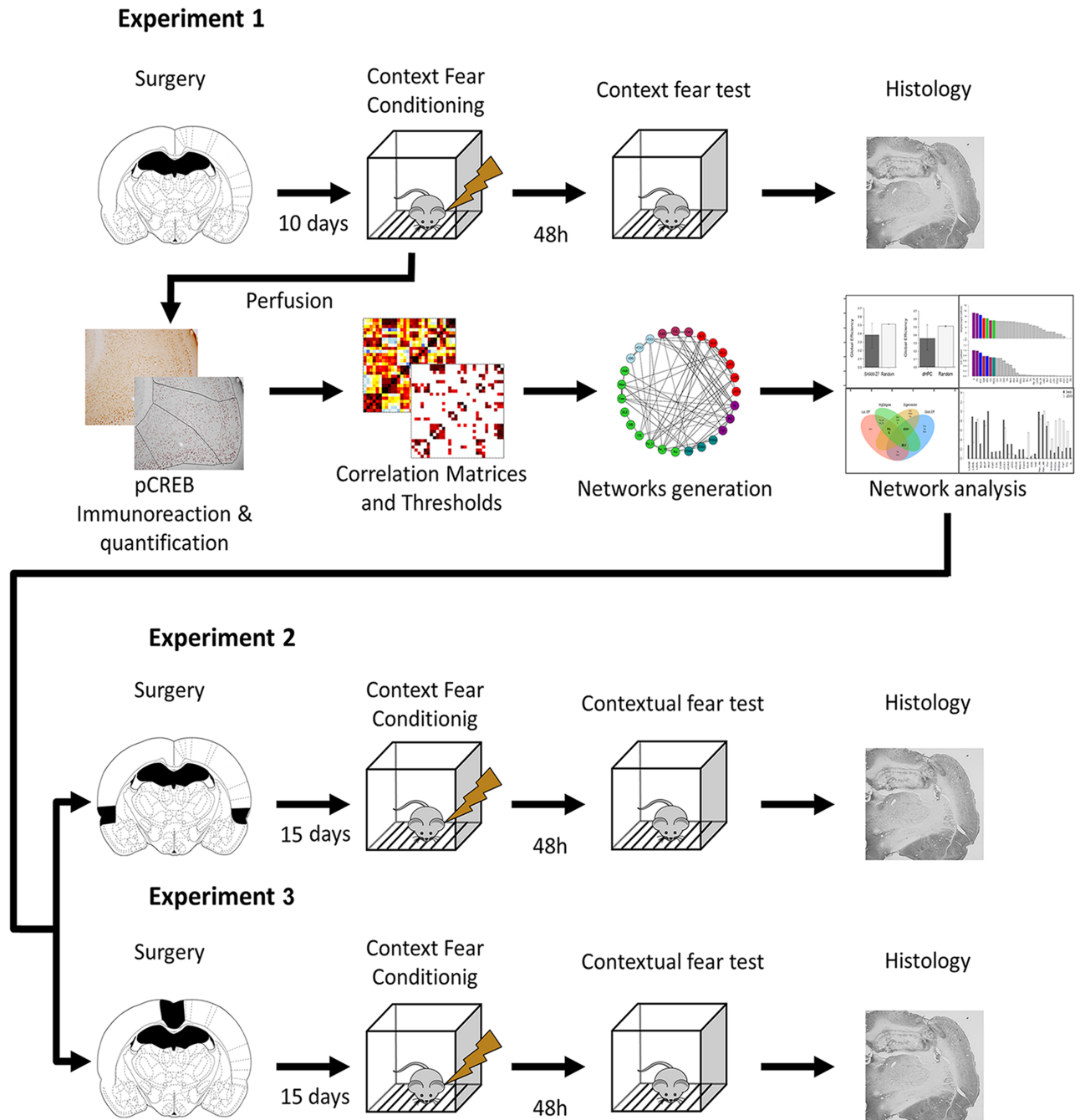


Fig 1. Overview of the experimental design. In Experiment 1, the rats underwent pre-training dHPC lesions and, after recovery, a CFC session. Half the sample underwent fear memory test 48 h later, whereas the other half was perfused 3 hours after CFC and had their brains processed and stained for pCREB protein. Thirty regions had their pCREB expression quantified and their pCREB inter-regional correlations computed. After thresholding the correlations, we analyzed the networks properties and compared them between the groups. Following network analysis, Experiments 2 and 3 employed double lesions to test if the network differences observed could be empirically supported.

<https://doi.org/10.1371/journal.pcbi.1006207.g001>

Multiple comparisons performed with p-corrected t-tests showed higher freezing time in both SHAM ($p = 0.0001$) and dHPC ($p = 0.0178$) groups compared to Imm group, but not statistically different from one another ($p = 0.4044$; Fig 3B). A KS test confirmed these results, showing no difference between SHAM and dHPC samples ($D_{24} = 0.3333$, $p = 0.2212$)

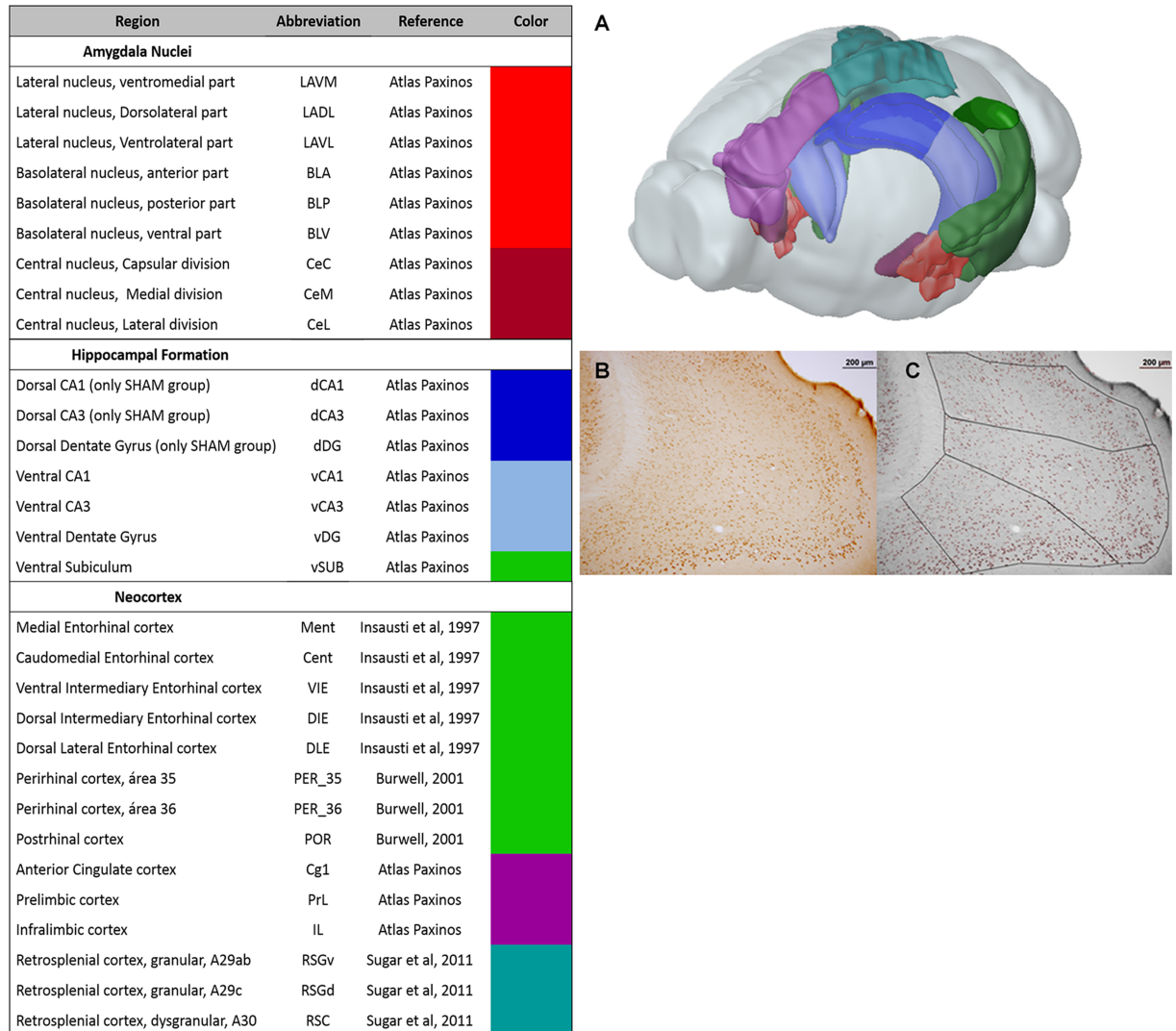


Fig 2. Regions included in Experiment 1. The columns show the name of each region, the abbreviations, the source of the anatomical definition adopted, and the color code used in the following figures for each group of regions. Color code—Red: basolateral complex of the amygdala; Dark Red: central amygdala nuclei; Blue: dorsal hippocampus; Light Blue: ventral hippocampus; Green: parahippocampal regions; Purple: prefrontal cortices; Magenta: retrosplenial cortices. A) 3D diagram of a rat brain showing anatomical localization of the included regions. Representative photomicrograph of a pCREB immunolabelled brain slice before (B) and after (C) nuclei quantification and region parcellation by CellProfiler. The scale bars indicate 200 μm .

<https://doi.org/10.1371/journal.pcbi.1006207.g002>

and both different from Imm group sample (SHAM: $D_{20} = 0.917$, $p = 0.0001$; dHPC: $D_{20} = 0.667$, $p = 0.0070$; Fig 3C). A Cohen's d showed a medium effect size between SHAM and dHPC means ($d = 0.630$) and large effect sizes between these two groups and Imm (SHAM: $d = 2.226$; dHPC: $d = 1.275$). These results show no effect of dHPC lesion in CFC learning and are in agreement with past studies [6]. To ensure the consistency of this lack of effect, we performed two additional experiments in which we test dHPC lesions in two paradigms that are known to be impaired by dHPC lesions (i.e. water maze and CFC with post-training dHPC lesions) followed by CFC with pre-training dHPC lesion (S1 Text). These experiments, which are replications of past studies [6, 31], confirm the consistency of this (lack of) effect.

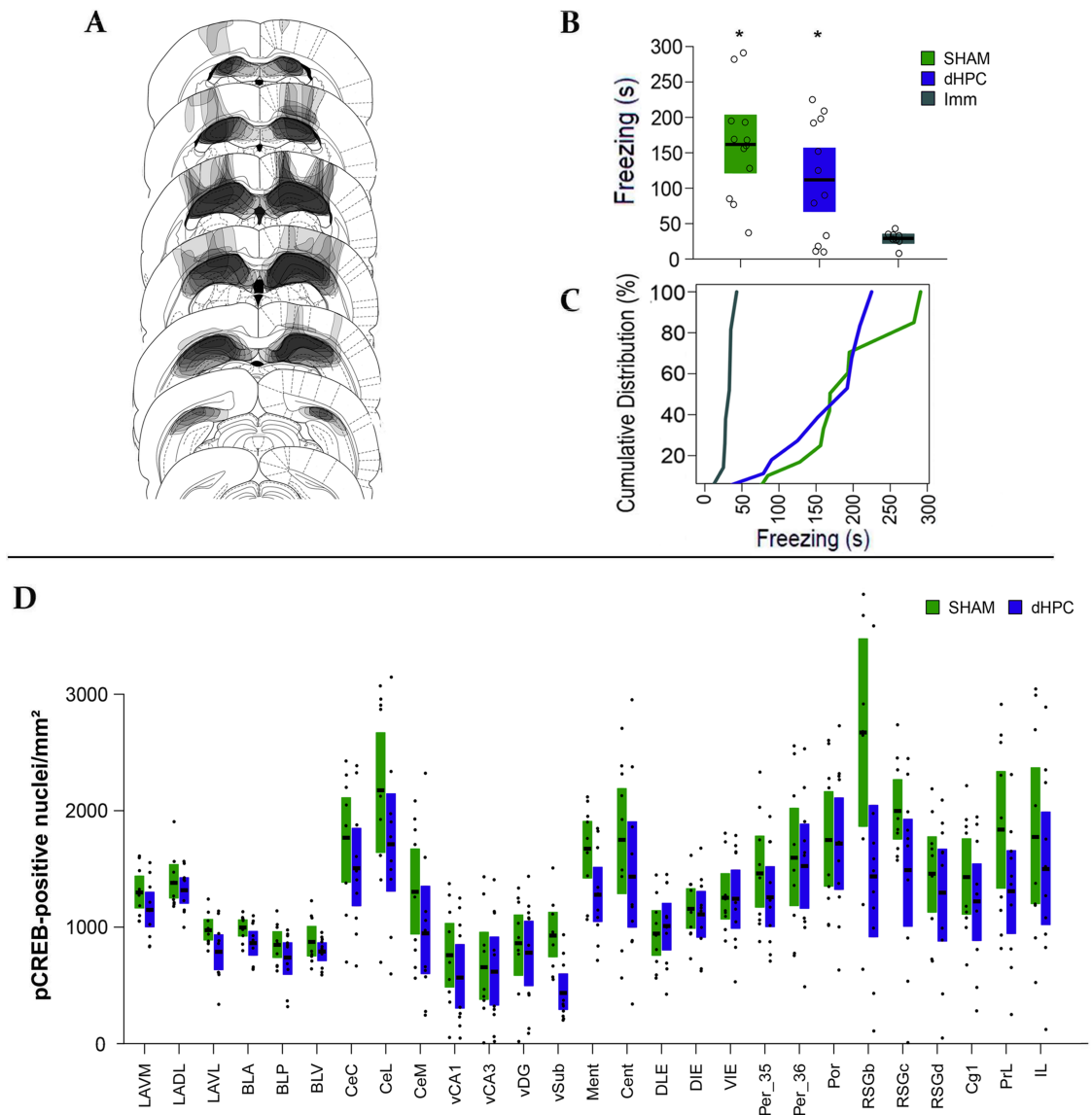


Fig 3. dHPC lesion does not impair CFC learning and memory. (A) Schematic diagram showing the distribution of the lesions in the dHPC group. (B) Mean (black line) and bootstrapped 95% CI of the Total Freezing Time during the five min context fear memory test of dHPC (N = 12), SHAM (N = 12) and Imm (N = 8) groups. The open circles show data distribution in each group. (C) Cumulative distribution of the sample as a function of Freezing Time showing the sample distributions. The “*” shows a significant difference from Imm at level of $p < 0.05$. (D) Mean (black line) and Bootstrapped 95% CI of the mean (boxplots) of the pCREB-positive nuclei density in each region and each group. The black dots show the data point distributions.

<https://doi.org/10.1371/journal.pcbi.1006207.g003>

dHPC damage does not alter the overall pCREB levels in the quantified regions

In the pCREB immunolabelling cohort, we tested whether the dHPC lesion altered pCREB expression after CFC learning in any of the studied regions by comparing the pCREB expression in each region between dHPC and SHAM groups. The Fig 3D shows the pCREB expression in each region and each group. The sample size in the pCREB expression cohort was 19 (SHAM: N = 9; dHPC: N = 10). We analyzed the pCREB-positive nuclei density by comparing each region between the groups using t-tests with bootstrap resampling. There was only

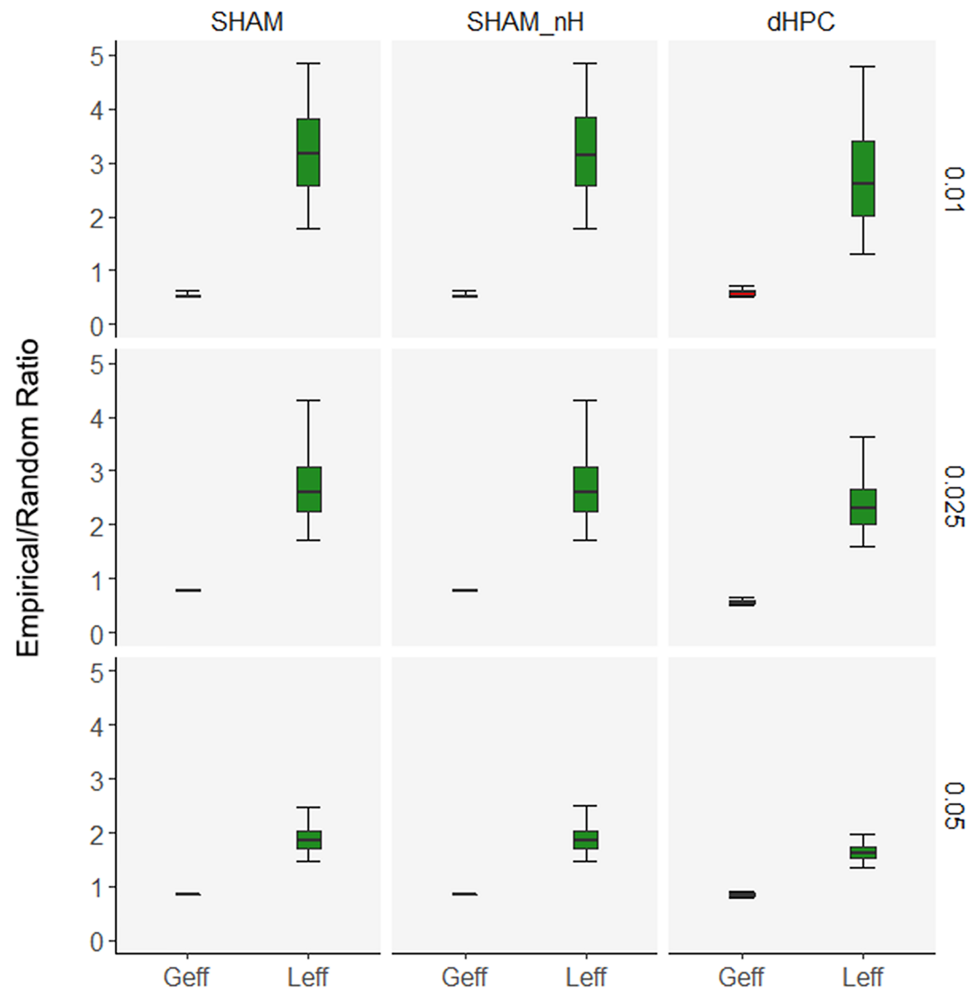


Fig 5. dHPC damage does not alter the CFC learning network small-worldness. Boxplots showing mean, lower and upper quartiles, and 95% CIs of the Empirical/Random ratio of Geff and mean Leff for the SHAM (left), SHAM-nH (center) and dHPC (right) networks and on the 0.05 (bottom), 0.025 (center) and 0.01 (top) thresholds. Small-world networks are expected to have Geff ratios around 1 (empirical and randomized networks have roughly the same values) and higher mean Leff ratios (higher empirical values than those of the randomized networks).

<https://doi.org/10.1371/journal.pcbi.1006207.g005>

The dHPC network had a bigger component in the 0.05 threshold, but fragmented into four components in the 0.025 and 0.01 thresholds (S1 Fig). Although in our study negative correlations were included as absolute values in the edge weights, no negative correlations survived the thresholds. Overall, the networks presented some visual differences in their pattern of connectivity, which we formally tested in the analyses that follow.

dHPC damage did not alter small-worldness of the CFC learning network

We first tested whether the empirical networks (SHAM, SHAM-nH and dHPC) were small-world by comparing their global (Geff) and local (Leff) efficiencies to those of randomized null hypothesis networks. We also tested if the dHPC lesion changed any of the efficiencies or the network small-worldness. The Fig 5 depicts the distribution of the empirical/randomized ratios of Geff and mean Leff for all networks and thresholds. In all cases, Geff ratios are roughly around 1, with a slight decay on the 0.01 threshold. Similarly, the mean Leff ratios are

consistently above 1, with the mean and upper range of ratios increasing as the threshold increased in rigor. Equivalent integration (Geff) and robustly higher segregation (Leff) values in empirical networks compared to randomized networks is consistent with small-world networks accounts [32, 33]. These results suggest that the networks engaged in CFC learning are small-world, which is in agreement with a previous work showing small-world organization in CFC retrieval networks [28]. Further, dHPC lesion did not seem to change the dHPC network small-worldness or its levels of Geff and mean Leff compared to the SHAM and SHAM-nH networks, suggesting that the overall characteristic interactivity in the dHPC network still benefit from small-world architecture.

dHPC network has alternative hubs

Hubs are defined as nodes positioned to confer the largest contributions to global network function, and are usually identified using multiple centrality metrics [24]. We considered as hub any region among the 25% most central regions in at least three of the four centrality metrics used (weighted degree, Wdg; eigenvector, Evc; closeness, Clo; and betweenness, Bet). Regions that were hubs across all thresholds were considered stable hubs. The Fig 6A and 6B shows the ranked centralities for the dHPC network and the metric intersection in the threshold 0.05 (S2–S4 Figs show all networks and thresholds). In this threshold, the SHAM network showed the regions IL and BLV as hub, whereas in the SHAM-nH the BLV and Por were hubs, and the dHPC network the hubs were the Per_36, Per_35, RSC and LAVL. The Fig 6C shows which regions were considered stable hubs across the thresholds, in each network. In the SHAM network, the IL was the only region identified as a stable hub across all thresholds. In the dHPC network, the RSC, and the Per_36 were stable hubs across all thresholds, and in the SHAM-nH network, no hub was stable across the three thresholds, but the IL was the most stable region (hub in the 0.025 and 0.01 thresholds), similar to the SHAM network. Employing connection-based and distance-based metrics to identify a hub makes more likely that the identified well-connected regions are also inter-region or inter-modular connectors. Noticeably, the dCA1 was in the upper quartile of both connection-based metrics, but not the distance-based ones, across the all thresholds (S2 Fig). These results suggest that different hubs emerged in the dHPC network. However, as the identification was descriptive, with no hypothesis test, it does not allow *a priori* interpretations regarding differences in the hub score between the networks. However, they are a first indication that there might be differences in the connectivity patterns between the SHAM and dHPC networks, as different regions emerged as hubs in these networks.

dHPC network hubs are associated to increased centrality measures

We addressed the hub score differences more formally and quantitatively by directly comparing the centralities between the groups in each region and each threshold using permutation test. The Fig 7 resumes the results of the permutation tests for each region, metric and threshold. Most importantly, we observed that the identified stable hubs were overall associated with significantly higher centrality levels in some metrics, comparing the dHPC SHAM-nH networks. In the dHPC network, the RSC showed significantly higher Wdg and Evc in all thresholds, and the Per_36 showed higher Evc levels in the 0.025 and 0.01 thresholds, compared to SHAM-nH network. In the SHAM-nH network, the IL showed higher Evc levels in the 0.025 and 0.01 thresholds, compared to the dHPC network (S5 Fig). Besides the stable hubs, some of the single-threshold or two-threshold hubs were also associated to significantly different centrality levels between the networks. In the dHPC network, the RSGd presented a higher Evc across all thresholds and a higher Wdg in the 0.025 and

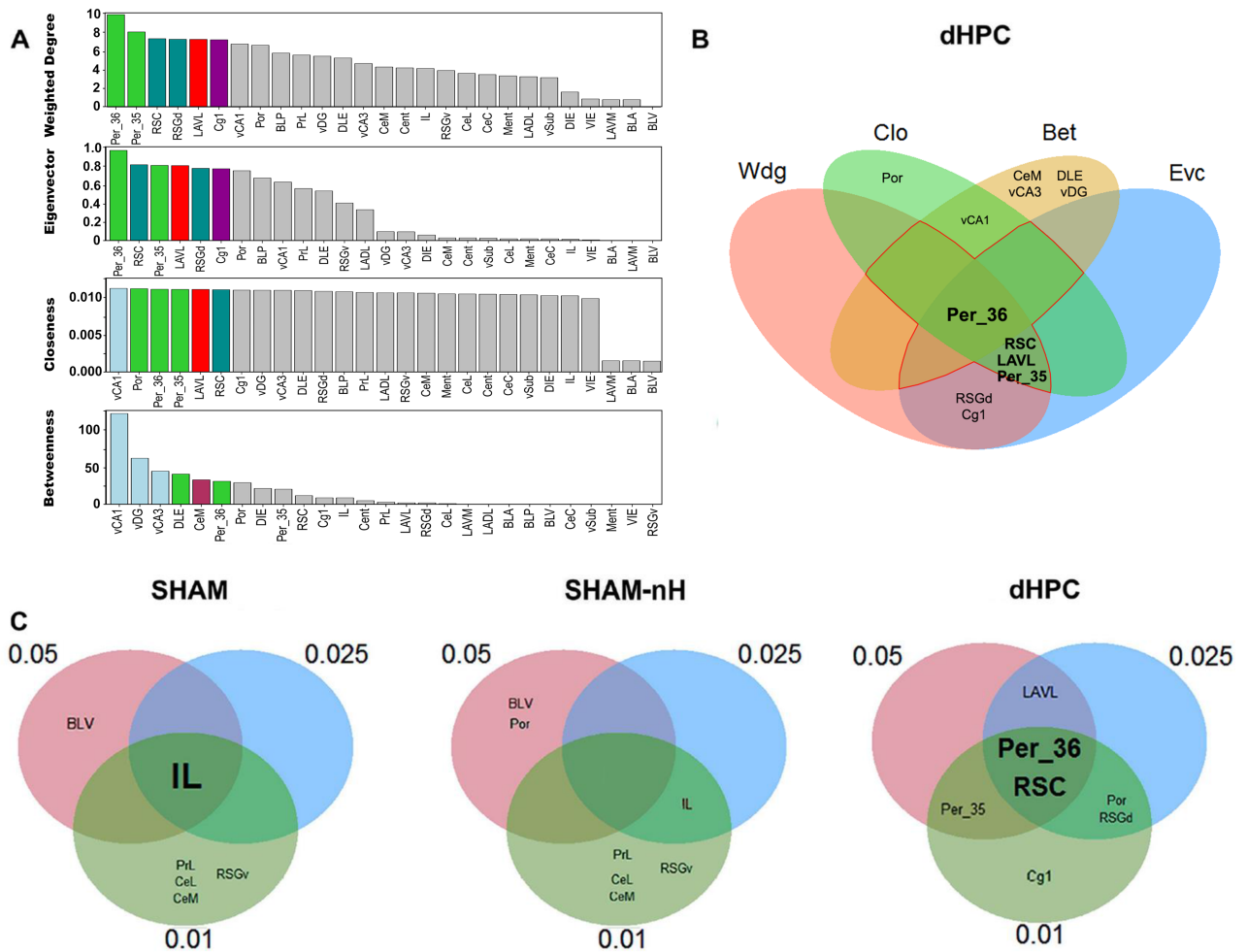


Fig 6. Hub identification of the networks. (A) The rankings of each centrality are shown for the dHPC network under the 0.05 threshold. The colored nodes are the upper 25% most central in each metric. (B) The intersections of the upper 25% most central regions of each metric are shown for the dHPC network under the 0.05 threshold. Any region within the overlapping area of at least three metrics was considered a network hub (inside the red perimeter). The hubs were identified in the networks with 0.025 and 0.01 thresholds as well (S2–S4 Figs), and the hubs of each threshold were intersected (C) to identify stable hubs across the thresholds in each network. Nodes are colored according to the code in Fig 2.

<https://doi.org/10.1371/journal.pcbi.1006207.g006>

0.01 thresholds. The LAVL had a higher Evc in the 0.025 threshold. In the SHAM-nH network, the BLV presented a higher Wdg across all thresholds, higher Bet in the 0.05 and the 0.01 thresholds, and higher Evc in the 0.05 threshold. Further, the CeM and PrL showed higher Evc, and the RSGv showed higher Bet, all in the 0.01 threshold. Some significant differences were present in non-hub regions such as BLP, vCA1, DLE and Por (higher metrics in dHPC network), and LAVM, BLA, and Por (higher metrics in the SHAM-nH network; S5 Fig). Lastly, some single-threshold hubs did not show significantly different centrality metrics in the thresholds they were considered hubs, such as LAVL, Per_35, Por and Cg1 (dHPC network) and CeL, Por (SHAM-nH network). These results provide evidence that when comparing SHAM-nH and dHPC networks, stable hubs in one network were associated to higher centrality levels relative to the other, and vice-versa. These results suggest that the CFC learning network under dHPC lesion has an increased dependence on its new hubs.

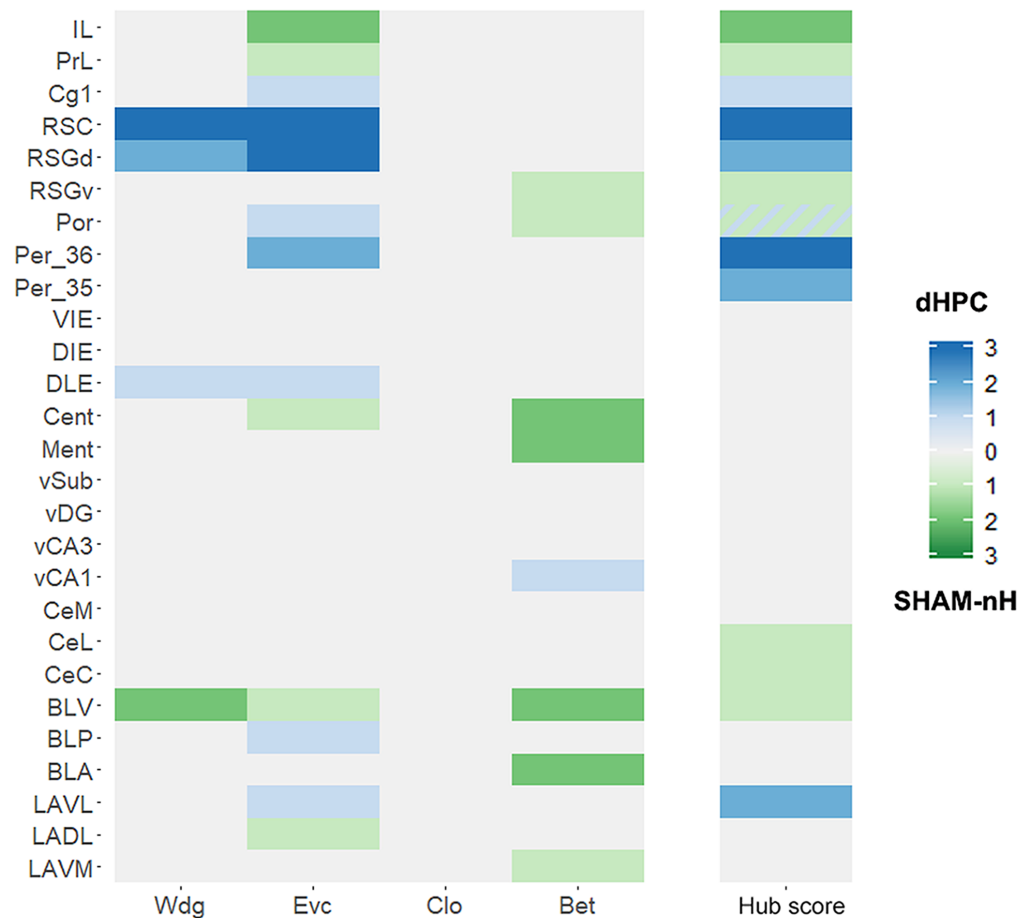


Fig 7. Centrality comparison between SHAM-nH and dHPC networks. The comparison was done for each region, centrality metric and threshold. Values in each cell show ranks of the amount of significant differences ($p < 0.05$ in the permutation test) across the thresholds in each region and metric, ranging from 0 to 3. The hub score column shows the amount of thresholds in which a region was considered a hub. Significantly higher centrality values and hub scores in the dHPC and SHAM networks are shown in shades of blue and green, respectively. If a region was hub in both networks, a stripped blue-green cell is shown with their respective gradient. It is possible to observe which hub scores are associated with significant differences in the centrality comparisons. The thresholds in which each difference and hub occurred is shown in S5 Fig. Wdg: Weighted Degree; Evc: Eigenvector; Clo: Closeness; Bet: Betweenness.

<https://doi.org/10.1371/journal.pcbi.1006207.g007>

dHPC damage changes interactions among other regions

The analysis so far focused on the nodes. We next examined edge (correlation coefficients) differences between the dHPC and SHAM-nH networks. First, we compared the distribution of correlations of each matrix between groups using a two-sample KS test. We observed significantly different correlation coefficient distributions between dHPC and SHAM-nH networks in all thresholds (**threshold 0.05**: $D_{151} = 0.2527$, $p = 0.0125$; **0.025**: $D_{106} = 0.3396$, $p = 0.0042$; **0.01**: $D_{67} = 4795$, $p = 0.0005$; Fig 8A and 8B and S6 Fig). Next, we compared each correlation coefficient between the groups. We computed the Z-score of the group difference for each correlation coefficient and considered a score of $|2|$ to be significant within the distribution. We observed 21 correlation differences with Z-scores above $|2|$ (Fig 8B). In nearly 2/3 of the significant differences (15 out of 21), the stronger correlation coefficients belonged to the SHAM-nH network, and 9 of them belonged to SHAM-nH hubs in that threshold; whereas only 6 differences the stronger correlation coefficient belonged to the dHPC network, one of which

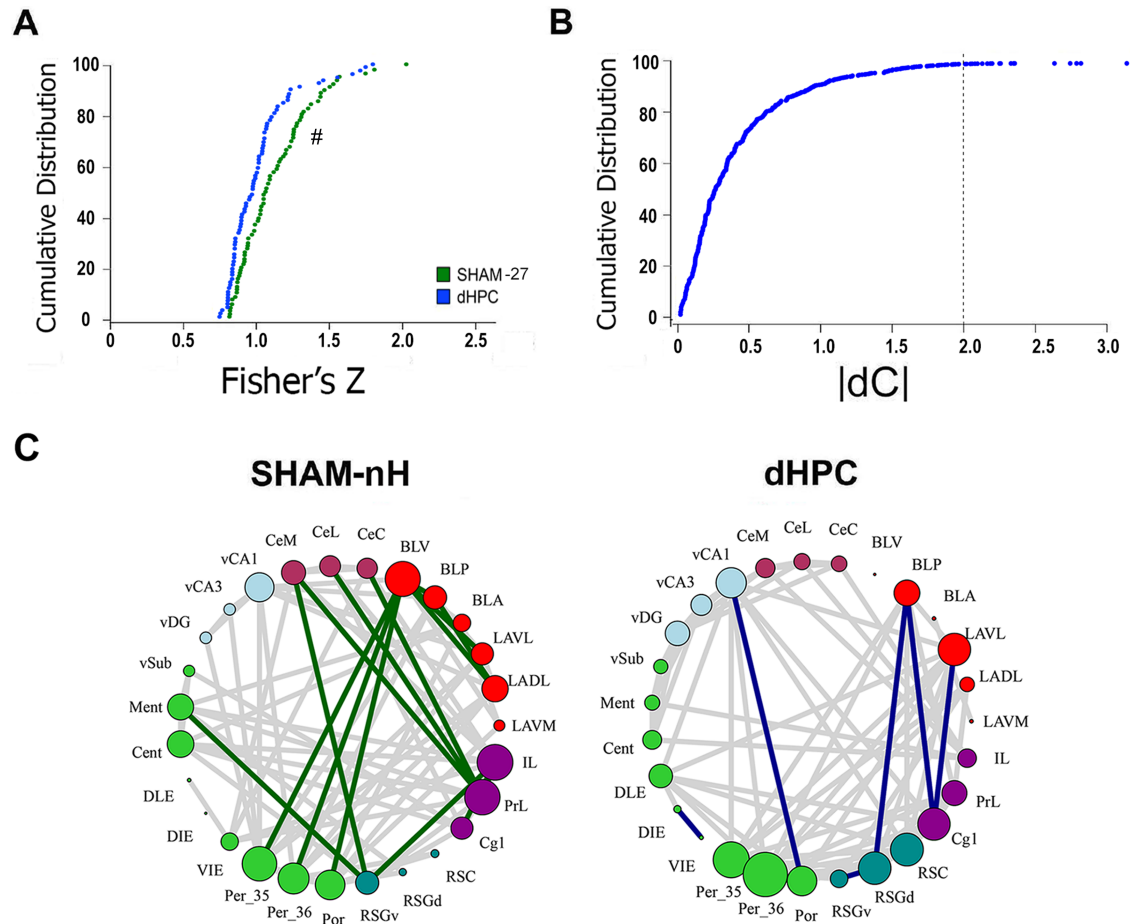


Fig 8. Connectivity change in dHPC network. (A) Cumulative distributions of the Fisher's Z transformed correlation coefficients from the SHAM-nH and dHPC matrices. The “#” indicates that these distributions are significantly different (Kolmogorov-Smirnov test, $p < 0.05$). (B) Cumulative distribution showing the z-score of the correlation coefficient differences between the groups. The dashed line shows the absolute Z-score of 2, revealing the values considered significant (beyond it) at the level of $\alpha = 0.05$. (C) The significantly different coefficients were plotted in each network, showing the network and nodes to which it belonged. The same procedure was performed in the 0.025 and 0.01 threshold networks and showed similar results [S6 Fig](#).

<https://doi.org/10.1371/journal.pcbi.1006207.g008>

belonged to a hub ([Fig 8C](#)). These results were similar across thresholds. In the 0.025 threshold, 19 out of 26 differences were higher in the SHAM-nH network (3 belonging to SHAM-nH hubs; [S6 Fig](#)), and in the 0.01 threshold, 20 out of 28 differences were higher in SHAM-nH network (9 belonging to SHAM-nH hubs). Overall, these results show that the SHAM-nH network presented a higher number of significantly stronger correlations compared to the dHPC network, many of which belonged to SHAM-nH hubs for that threshold.

The different correlation distributions and the differences in correlation strengths between the networks add support to the hypothesis of different connectivity patterns in the dHPC network. Further, it suggests that dHPC indirectly influences interactions between other regions, most of which were observed to be weakened.

Damaging the dHPC network Hubs

The network analysis revealed some differences between the dHPC and the SHAM (or SHAM-nH) networks. Particularly, the alternative hubs emerging in the dHPC network (Per_36 and RSC) and their statistically higher centralities compared to the SHAM-nH

network suggest that these regions may increase in their importance to CFC learning in the absence of hippocampus. We empirically tested this hypothesis in the next two experiments by damaging both the dHPC and one of these hubs pre-training to CFC. Our hypothesis is whether further insult to the network would compromise the necessary structure of the network to promote CFC learning.

Experiment 2—Pre-training dHPC-Per double lesion does not impair CFC

In Experiment 2, because it was technically difficult to damage specifically the Per₃₆ and most animals had a significant part of the Per₃₅ damaged, we considered animals with lesions extending to both Per₃₆ and Per₃₅, denominating it Per. Henceforth, Per will be mentioned when Per₃₅ and Per₃₆ are considered together. During histological analysis, we excluded four rats from the dHPC-Per, two from the Per and one from the dHPC groups due to either extensive bilateral lesions to the regions surrounding Per (Temporal, Auditory, Parietal, Visual cortices, ventral CA1 or Lateral Amygdala), or no detectable dHPC and/or Per cellular loss in most slices examined. The final sample in this experiment was 38 (SHAM, dHPC and Per: N = 10/each; dHPC-Per: N = 8). In the remaining sample, cellular loss was mostly confined to the Per₃₆, Per₃₅ and to dHPC. In the dHPC and dHPC-Per groups, slight occasional damage was observed in the secondary Visual and Medial Parietal cortices overlying dHPC due to needle insertion (Fig 9A). In the behavioral analysis, the bootstrapped ANOVA showed no group difference ($F = 0.842$, $p = 0.479$; Fig 9B and 9C). The KS test showed no significant differences among groups' distributions and the Cohen's d values did not show any considerable effect size (Fig 9 bottom). These results indicate that neither Per or dHPC-Per lesions affect CFC learning and memory.

Previous studies observed no pre-training Per lesion effect on CFC [34, 35], despite some contradictory evidence [36]. Our results support the hypothesis that pre-training Per and dHPC-Per lesions do not affect CFC learning and memory.

Experiment 3—Pre-training dHPC-RSC double lesion impairs CFC

During histological analysis, three rats from the RSC and one from the dHPC-RSC group were excluded from the analysis due to non-detectable cellular loss in most slices. The final sample in this experiment was 39 (SHAM: N = 10, dHPC and RSC: N = 9/each, dHPC-RSC: N = 11). The lesions affected mainly the dHPC and RSC, with frequent lesions to RSGd and occasional minor unilateral lesions of RSGv and secondary visual cortex. In the behavior analysis, the bootstrapped ANOVA revealed a main effect of group ($F_{3,35} = 3.691$, $p = 0.01975$), which the p -corrected t tests showed to be due to a lower freezing in the dHPC-RSC compared to that of the SHAM group ($t_{20} = 3.315$, $p = 0.0270$; Fig 10B and 10C). No other significant differences were observed. This result was further confirmed by the KS test, which revealed significantly different distributions between the dHPC-RSC and the SHAM samples ($D = 0.609$, $p = 0.0303$). No other differences were observed (SHAM vs dHPC: $D = 0.378$, $p = 0.330$; SHAM vs RSC: $D = 0.367$, $p = 0.377$; dHPC vs RSC: $D = 0.333$, $p = 0.316$; dHPC vs dHPC-Per: $D = 0.485$, $p = 0.098$; Per vs dHPC-Per: $D = 0.374$, $p = 0.289$). The Cohen's d values also confirmed the above results showing a large effect size between SHAM and dHPC-RSC means ($d = 1.469$). Lesser effect size values were observed in the other comparisons (SHAM vs dHPC: $d = 0.463$; SHAM vs RSC: $d = 0.75$; dHPC vs Per: $d = 0.338$; dHPC vs dHPC-Per: $d = 1.056$; Per vs dHPC-Per: $d = 0.598$; Fig 10 bottom), although the effect size between dHPC and dHPC-RSC was somewhat large. These results show that both dHPC and RSC contribute to CFC learning, although single lesion of these regions was not sufficient to impair CFC.

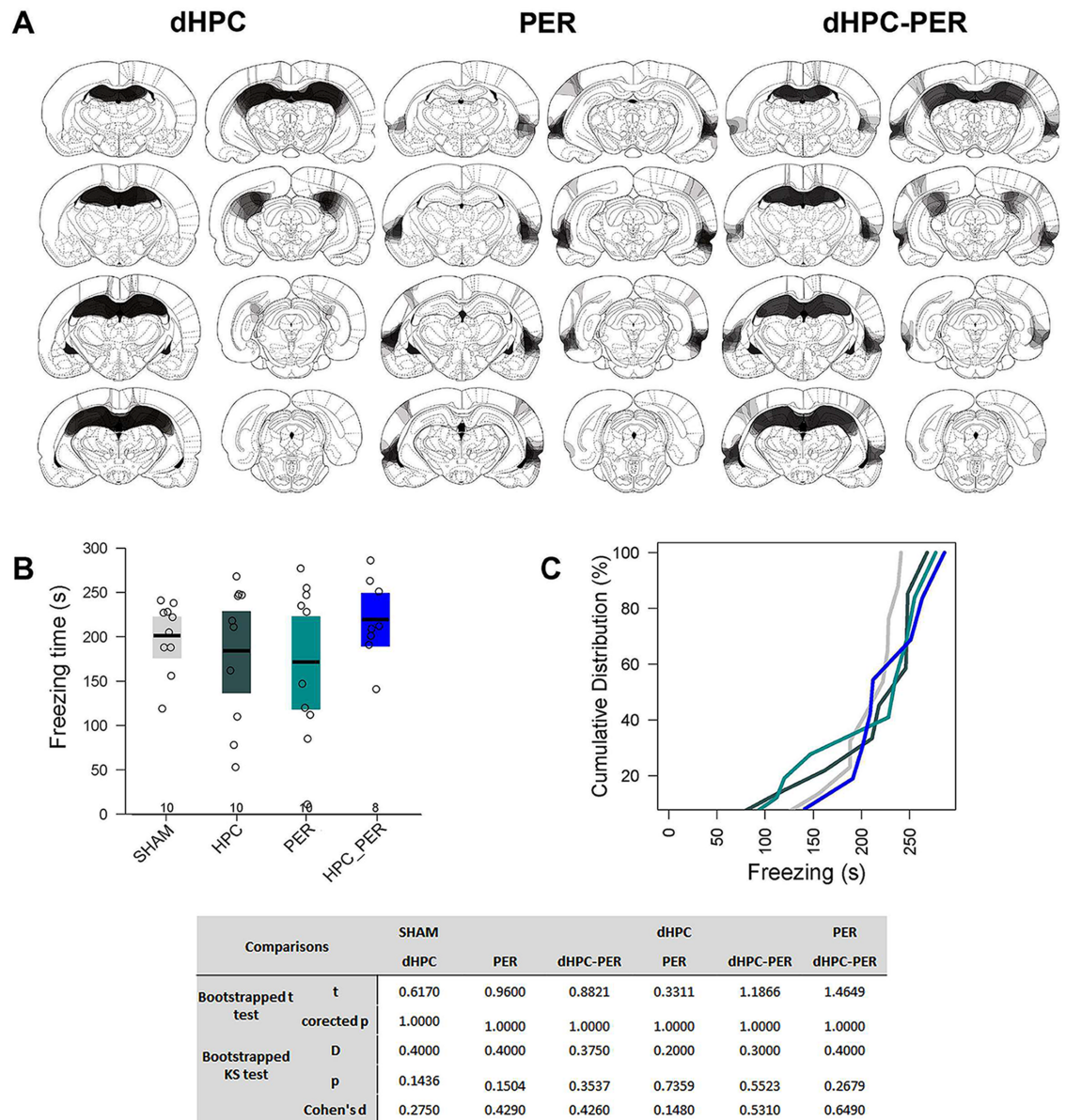


Fig 9. Per and dHPC-Per lesions on CFC learning. (A) Histological diagrams showing the distribution of areas damaged in dHPC, Per and dHPC-Per groups. The more overlapped the damaged areas across subjects, the darker the area. (B) Mean and bootstrapped 95% IC of the total freezing time in SHAM, dHPC, Per and dHPC-Per groups during 5 min of CFC memory test. Dots show the sample distribution of each group. (C) Cumulative distribution of the total freezing time in each group in the same CFC memory test. The bottom table shows all the statistical tests performed and the corrected p-value for each comparison.

<https://doi.org/10.1371/journal.pcbi.1006207.g009>

Further, it supports the network analysis in Experiment 1 that RSC becomes a key region in the dHPC network engaged in CFC learning.

However, a careful analysis of the lesion extensions raises two possible alternative explanations for the observed results. First, the RSC lesion extension seems to be larger in the dHPC_RSC group than in the RSC group, which raises the possibility of the unimpaired behavior in the RSC be due to a smaller lesion. Second, as lesion frequently extended to RSGd in the dHPC_RSC group, there is the possibility that RSGd lesion had an effect in the impaired behavior observed in this group.

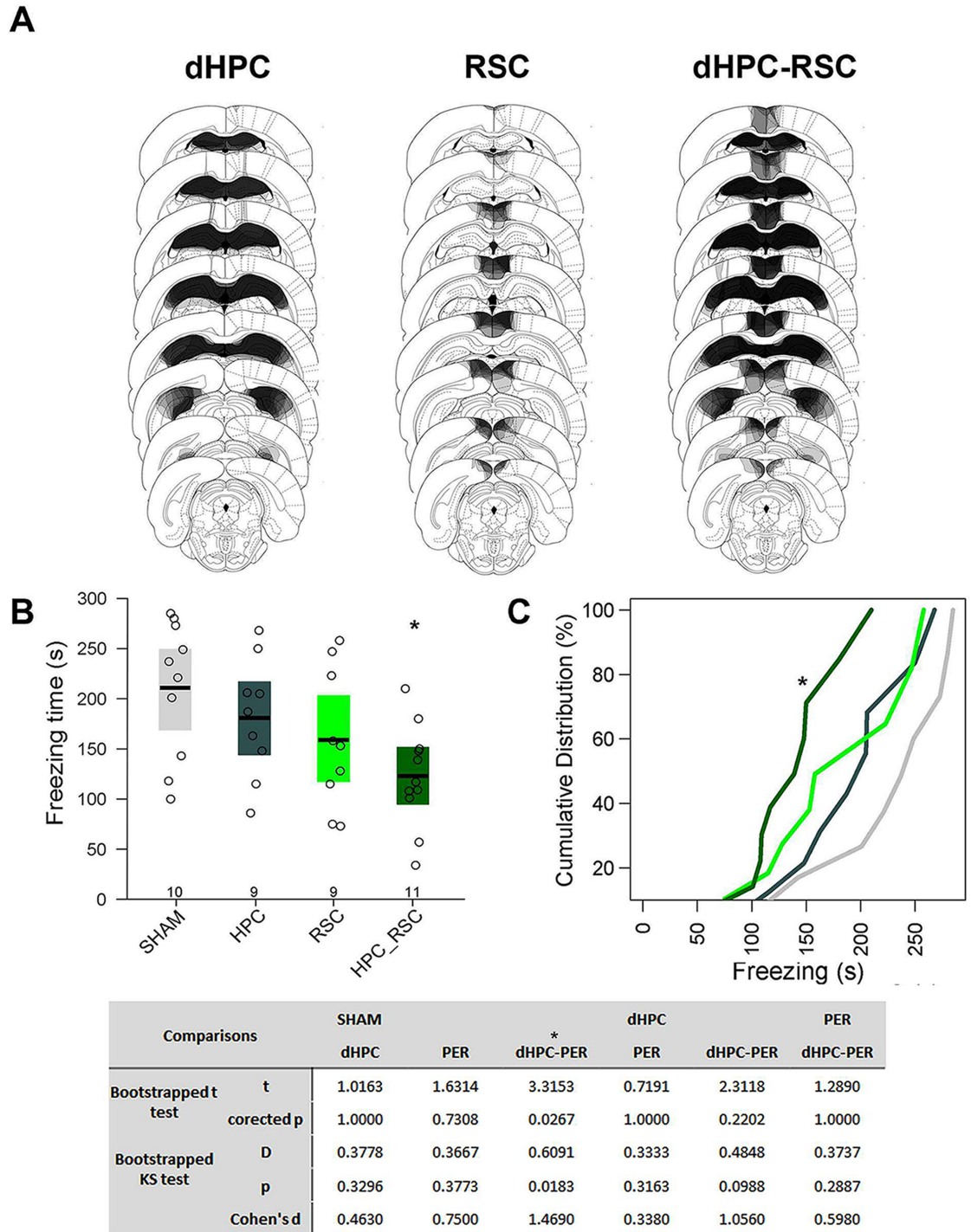


Fig 10. RSC and dHPC-RSC lesions on CFC learning. (A) Histological diagrams showing the distribution of areas damaged in dHPC, RSC and dHPC-RSC groups. The more overlapped the damaged areas across subjects, the darker the area. (B) Mean and bootstrapped 95% IC of the total freezing time in SHAM, dHPC, RSC and dHPC-RSC groups during 5 min of CFC memory test. Dots show the sample distribution of each group. (C) Cumulative distribution of the total freezing time in each group in the same CFC memory test. The bottom table shows all the statistical tests performed and the corrected p-value for each comparison. “*” shows significant differences relative to SHAM group (corrected-p < 0.05).

<https://doi.org/10.1371/journal.pcbi.1006207.g010>

To test the first alternative possibility, we measured the percentage of lesion in the dHPC, RSC and RSGd regions in the RSC and dHPC_RSC groups, and compared them between these groups. A t test with bootstrap resampling showed that the RSC and RSGd lesion extensions were, in fact, larger in the dHPC_RSC group than in RSC group (RSC: $t = 2.252$, $p = 0.042$; RSGd: $t = 2.582$, $p = 0.021$; [S7A Fig](#)). Next, we tested whether this difference in the lesion extension had any influence in the observed behavior. We compared the freezing among the groups just as above using the percentage of damage as co-variables by an ANCOVA. The ANCOVA still showed the group main effect ($F_{3, 32} = 3.777$, $p = 0.0199$), but none of the lesion extensions showed any co-varying effect (**RSC**: $F_{1,32} = 0.872$, $p = 0.3575$; **RSGd**: $F_{1,32} = 0.001$, $p = 0.9728$; **dHPC**: $F_{1,32} = 2.937$, $p = 0.0962$). These results suggest that the lesion extension of these regions had no effect on the observed behavior. One thing to be considered however, is that both RSC and dHPC had a minimum of 50% of damage because of our exclusionary data. We do not rule out the possibility that, in an unbiased sample, there could be a relation between lesion extension and behavior, but this relation seems not to be evident when lesion extension exceeds 50% of the target regions. Therefore, it is unlikely that the lack of effect in the RSC group could have been due to the observed smaller RSC lesion observed in the group in comparison to the dHPC_RSC group.

To address the second possibility, we selected dHPC_RSC individuals that had their lesions more constrained to the RSC, with minor to undetectable damage to RSGd (less than 30%, $N = 4$), and compared them to the other groups. If the dHPC and RSC double lesions have an effect that is independent from the RSGd lesions, the differences observed should still be observable. Bootstrapped t tests showed a lower freezing time in the strict dHPC_RSC subgroup compared to the SHAM group ($t_{13} = 2.532$, $p = 0.049$), whereas it did not differ from any of the other groups (dHPC: $t_{12} = 1.717$, $p = 0.135$; RSC: $t_{12} = 0.992$, $p = 0.349$; dHPC_RSC: $t_{14} = 0.024$, $p = 0.971$; [S7B Fig](#)). These results replicate the results above where samples included significant RSGd damage, suggesting that double lesions of the dHPC and RSC impair CFC learning and memory independently of the RSGd damage. It is important to note, however, that the RSGd presented almost as many higher centrality values as the RSC in the dHPC network compared to the SHAM-nH network. Thus, we do not rule out the possibility of RSGd also possesses some increased influence in the dHPC network and in the behavior.

Discussion

The present study employed network science to investigate CFC learning in dHPC-damaged rats. A fair amount of studies have observed CFC learning in absence of dHPC [[6](#), [12](#), [13](#)], but no evidence had been provided regarding how the remaining brain systems can support CFC learning without hippocampus. Our study shows four main findings. First, we found that the CFC learning network under dHPC damage did not affect the small-worldness observed in the SHAM and SHAM-nH networks, and presented comparable levels of global and local efficiencies to the SHAM network. Second, we identified different hubs in each network, which were associated with different centrality levels between the dHPC and SHAM-nH networks. Third, differences in correlation coefficients distribution and strength suggest that dHPC indirectly influence interactions throughout the network. Fourth, by damaging the regions identified as hubs in the dHPC network, we showed that double lesion of dHPC and RSC, but not dHPC and Per, disrupt CFC learning and memory. Overall, despite the unaltered topology, dHPC network was sufficiently different such that alternative hubs emerged.

Many studies have observed small-world architecture in both anatomical and functional brain networks [[37](#), [38](#)]. Small-world architecture is proposed to confer optimized cost-efficiency of connections for information flow [[39](#)]; as well as protection to central regions to

targeted attack, when compared to other topologies [i.e. scale free networks; 21]. Further, computational studies suggest that the concomitant high local processing and integration across distributed clusters provided by small-world networks can support information processing [40]. This is in accordance with empirical studies in somatosensory neuronal networks, which maintain their small-worldness both at ‘rest’ and after stimulation, despite the enhanced interactivity among clusters [41]. Conserved small-worldness with increased levels of integration was also observed in human studies investigating network reconfigurations during motor learning [42], working memory [43], successful visual discrimination [44], recollection [45], and emotional and motivational experiences [23]. In our study, showing that dHPC lesion did not change *Geff*, *Leff* levels nor small-worldness was informative as it is in accordance with the observed performance. The unimpaired behavior and unchanged small-world and efficiencies in the dHPC group suggest that the network still maintain an interactivity capable of supporting CFC learning.

In the present study, the RSC and Per_36 showed stable hubness in the dHPC network and presented higher centrality levels compared to SHAM-nH network. These regions are deemed as central components of the proposed antero-temporal (AT, Per_36) and postero-medial (PM, RSC) memory systems that converge to the hippocampus [46], suggesting that dHPC damage increases the importance of the ‘upstream’ regions. Albeit the validation experiments showed impaired CFC memory only in the dHPC-RSC double lesions, but not dHPC-Per, the centrality comparison supports this double lesion data. The RSC displayed more robust centrality differences, with significance in more metrics and in all thresholds. These stable centrality differences may be reflecting an increased demand over—and dependence on—the RSC in the dHPC network.

Our data also corroborates the current framework of Per and retrosplenial cortex (RSG) functions. The Per is related to recognition, affective processing and associative memory of non-spatially referenced cues [47–49], whereas the RSG is important for processing spatial, contextual information and episodic memory [46, 50]. Therefore, it is parsimonious that the CFC network under dHPC damage be more dependent on RSG than on Per.

The RSG has been considered an anatomical connector of the diencephalon, medial temporal lobe and cortices implicated in anterograde amnesia [2, 51]. A recent re-emerged interest in the RSG provided a diverse number of evidences highlighting its function. For instance, studies in humans showed increased activity in RSG for stable landmarks when navigating in virtual reality environments [52–54]. Studies in animal models provided evidence that RSG integrates, encodes and stores spatial information [55–57], that it is necessary during spatial navigation [58, 59] and context fear learning and memory [60–62]. This framework suggests that the RSG is an important component of spatial learning and memory systems. Furthermore, RSG is highly interactive with regions known to be involved in spatial and contextual learning such as hippocampus [63] and Por [64]. The present results are in line with these findings and suggest that in dHPC absence, contextual learning networks might increase their dependence over the RSG.

On a different perspective, increased activation and functional connectivity are hallmarks in patients with traumatic brain injury [TBI; 65]. In resting-state fMRI, regions exhibiting increased connectivity generally compose network rich clubs, which include the RSG and Per [regions defined as PCC, and ParaHipp, respectively; 65, 66]. Although our data is specific to CFC learning after dHPC lesion, our findings are in line with the human evidence of increased connectivity of RSG and Per after brain injury. There has been some evidence of a positive relationship between the increased functional connectivity in the pre-frontal cortex and behavior (i.e. working memory), which has generally been interpreted as an adaptive compensation [67–69]. However, this positive relationship was also observed to not be maintained after

sustained working memory practice, despite the maintained increased functional connectivity during the task [70]. In fact, increased functional connectivity and inefficient behavioral performance is very often observed [71, 72], conflicting with the compensation account. Another account proposes that the ‘hyperconnectivity’ observed after brain injury expresses an overload in the alternative reminiscent pathways still capable of supplying the cognitive demand under a “challenged” circumstance [25, 73]. According to the hyperconnectivity account, performance can be impaired or not depending on the cognitive demand of the task and the level of overload in the reminiscent pathways. The relationship between behavior and increased functional connectivity (i.e. centrality levels) in RSG in our double lesion experiments could be interpreted as evidence for a compensatory account. However, CFC is a very brief experience and, although we did not evaluate dHPC networks over time or after multiple experiences, other studies observed decrease of memory across time [13] and certain conditions that yield an impaired behavior, interpreted as a less efficient learning [6]. Our results complement the existing evidence of CFC learning after dHPC loss and help shape a framework that is in accordance with the hyperconnectivity account.

We also observed an indirect influence of dHPC lesion on interactions among other regions, which is consistent with both simulation of functional brain activity under brain damage [74], and studies on unilateral focal brain lesions [75, 76]. This non-local alteration in connectivity was associated with behavioral impairments in patients. Although we did not observe a contextual fear memory impairment, the altered pattern of connectivity observed gives support to a partially different CFC learning network under dHPC damage, and suggests that what is learned (associated to the shock) might be different under dHPC lesion.

Importantly, the lack of effect on pre-training lesions involving Per should not be taken as evidence against its involvement in CFC. As RSC and Per in this study, pre-training hippocampal lesions do not impair CFC either, under most conditions [6]. Further, post-training lesions to all these regions resulted in impaired CFC memory [6, 36, 61, 77] and after pharmacological manipulations [8, 78, 79], evidencing that these regions do play a role in CFC. Our hypothesis was focused on whether CFC learning would still be supported after further targeted network damage.

Moreover, previous studies employing pre-training single lesions on both Per and RSG have reported conflicting results regarding their effect on CFC. On Per lesions, one study reported impaired CFC memory in Per-damaged animals [36], whereas other reports did not find impairment [34, 35]. These studies employed different lesion methods and behavioral parameters, rendering it difficult to point a source of the discrepancy. Although the present study employed methods closer to that of Bucci and colleagues (2000), the conflicting results remain. Regarding RSG, Keene and Bucci [60, 80] have consistently observed impaired CFC memory in pre-training RSG lesions, whereas another study did not find such impairment [81]. Our procedures were as similar as possible to that of Keene and Bucci [60], however, we aimed for the RSC instead of the whole RSG. Although we did damage portions of RSGd in some animals it is possible that our lack of effect on RSC single lesions was due to not damaging the whole RSG. Alternatively, it is possible that Per and RSG single lesions may be at least partially compensated just as dHPC lesions, resulting in higher rates of mixed results due to a less effective learning [12].

Despite the unimpaired behavior in dHPC-damaged animals, it is very likely that the contextual information learned is different [3, 14]. Some authors discussed about the complexity of the CS under hippocampal damage [11, 12], however, clearly assessing the content learned as CS in CFC preparations remains as a limitation. Findings from tasks that allow a better assessment of the learned content strongly suggest that both Per and RSG support configural learning—defined as complex stimuli bound together in a stimulus-stimulus manner. For

instance, Per-damaged rodents have impaired complex visual discrimination tasks [82, 83], and RSG-damaged rodents have impaired spatial memory in tasks in which spatial cues moved between trials [84, 85]. Further, RSG was shown to integrate distributed spatial information across delimiting marks [55]. These data suggest that RSC and Per can support some configural learning in dHPC-damaged animals. This is supported by studies employing whole-hippocampus damage and complex maze tasks [86].

Methodological considerations and limitations

There are some points about the present study that need attention when interpreting the results. First, we do not show both behavioral and brain activation data in the same subjects in Experiment 1, therefore not directly showing that the altered brain networks are linked to preserved CFC learning. The purpose of our study was to investigate how learning and memory formation about CFC occurs in the absence of the dHPC, however, a limitation of the imaging methods used in rodents to assess experience-driven proxies of brain activation (i.e. IEGs such as *c-fos* and *arc*) is that they are acquired post-mortem and, thus, require to be the last step in the experimental design. Previous studies used post-retrieval IEG acquisition in order to acquire both brain and behavior data from the same subjects [28]. However, such design would need us to assume that brain activation during CFC learning and retrieval are equivalent, which there is evidence showing the contrary [87, 88]. Further, IEGs and pCREB expressions are primarily related to neuronal plasticity processes [30], and acquiring post-retrieval pCREB expression would not necessarily reflect a measure brain activation during retrieval, but possibly processes that could induce ‘post-retrieval plasticity’ [i.e. new encoding, reconsolidation; 89]. Given this limitation, we ensured that our brain network and behavior results are not product of variability by doing additional experiments challenging this hypothesis. Our Experiments 2 and 3 test whether the network analysis could be a product of chance (variability included), and we ran two additional experiments that replicate previous studies [5, 6] showing paradigms impaired by dHPC lesion followed by unimpaired CFC in rats with pre-training dHPC lesions (S1 Text). Despite this caveat, the confirmation experiments show the consistency of our observations and the relation between the altered brain networks and preserved CFC learning in dHPC damaged rats.

Second, when comparing networks, one seeks differences attributable solely to the network structure, but network attributes such as number of nodes, edge density and mean degree might add confounding effects if they are not equivalent between the networks. However, altering networks so that they match in these attributes (ex. proportional thresholding, node removal) might change the network topology and drive false positive and/or negative differences [90]. As no formal solution exists for comparing networks of differing sizes, in our study, we removed nodes from the SHAM network (producing SHAM-nH) in order to compare it to dHPC network. This node removal did not affect the overall network topology or its small-worldness (Fig 5), minimizing possible biases from this procedure. Additionally, the thresholds applied in the present study intended to remove correlations that were no different from chance, which depended solely on the pCREB co-variation among the regions within each condition. Therefore, there was no proportional thresholding to control edge density and mean degree across conditions. The fact that we did observe equivalent edge densities across conditions was due to their similar co-variations. This characteristic reflected in our analysis (similar efficiencies) and can be observed when plotting the networks based on Euclidean distances (S1 Fig). Importantly, the thresholding could have produced networks with differing edge densities or mean degree, which would require alternative approaches to the analysis.

Third, the lesion method used in Experiment 1 (electrolytic lesion) does not spare fibers of passage, which may have affected connections between other regions. Whilst this could have altered the network more than intended, the behavior data suggests that the network is likely to contain the elements required in CFC learning and memory since no impairment was observed. Furthermore, the networks studied here, which are based on pCREB expression, identified similar hubs to recent anatomical studies based on larger tract-tracing databases [91, 92], making a confounding effect of fiber lesion unlikely.

Fourth, the Experiment 1 differs from Experiments 2 and 3 in number of shocks during the training session. Single shock CFC sessions is generally a weaker experience and tend to yield more variable levels of behavior. We used the three shocks procedure to ensure a robust performance level in Experiments 2–3 such that impairments would be more detectable. Additionally, the performances of SHAM controls and dHPC groups were very similar, ruling out the possibility of a ‘hidden’ memory impairment in the dHPC group in Experiment 1.

Conclusion

There is growing interest in the use of network approaches to predict cognitive performance from brain imaging data [22, 44, 45]. However, formally testing predictions in human experimentation is still a challenge called for attention [93]. We applied network analysis in rodent models and were able to empirically test the validity of these models subsequently. We found that CFC network under dHPC damage increase its dependence on new hubs, and further damaging these new hubs may compromise the formation of the functional network necessary for CFC learning and memory. Future employment of finer techniques (i.e. optogenetics, transgenic animals) may provide sophisticated ways to test network predictions.

Materials and methods

Subjects

A hundred and thirty nine male Wistar rats weighting 300-370g were obtained from the university vivarium (CEDEME, SP). They were housed in groups of 4–5 and maintained on a 12h light/dark cycle, room temperature of $22 \pm 2^\circ\text{C}$, with free access to food and water.

Ethics statement

This research made use of one hundred and thirty nine male Wistar rats obtained from the university vivarium (CEDEME, SP). All experiments were approved by the University Committee of Ethics in Animal Research (CEUA, approval numbers #0392/10, #409649 and #7683270116). The guidelines used by CEUA are in accordance with National Institutes of Health Guide for the Care and Use of Laboratory Animals in the USA.

The present study involved stereotaxic surgeries. In these procedures, the rats were anesthetized with Ketamine (90mg/kg, Ceva, Paulínia, Brazil) and Xilazine (50mg/kg, Ceva, Paulínia, Brazil) given in intraperitoneal injections. In the end of the behavioral procedures, the rats were anesthetized with 10% chloral hydrate and perfused transcardially with 4% paraformaldehyde.

Surgery

The rats were anesthetized with Ketamine (90mg/kg, Ceva, Paulínia, Brazil) and Xilazine (50mg/kg, Ceva, Paulínia, Brazil), and mounted into a stereotaxic frame (David Kopf Instruments, Tujunga, CA). Each animal had their scalp incised, retracted and the bregma and lambda horizontally adjusted to the same plane. Small holes were drilled in the skull in the

appropriate sites. The rats received bilateral electrolytic lesions in the dHPC by an anodic current (2 mA, 20 s) passed through a stainless steel electrode insulated except for about 0.7 mm at the tip. The following coordinates were used: - 4.0 mm from bregma (AP), ± 2.0 and ± 4.0 mm from the midline (ML) and -3.6 mm from the skull surface (DV). Control (SHAM) animals underwent the same procedure except that they did not receive currents. After the surgery, the rats received antibiotic and diclofenac intramuscularly (3mg/kg, Zoetis, Madison, NJ) and were allowed to recover for 15 days. To avoid corneal lesions associated to the anesthetic used, the rats had their eyes hydrated with ophthalmic gel (Bausch & Lomb, Rochester, NY) and received a post-surgery injection of yohimbine (2mg/kg, Sigma, St. Louis, MO).

In Experiment 2 the surgeries were performed as above, but the rats received bilateral neurotoxic lesions in the dHPC, Perirhinal cortex (Per), both (dHPC-Per) or SHAMs. The lesions were made by N-methyl-D-aspartic acid (NMDA, 20 mg/ml in 0.1 M phosphate buffered saline, pH 7.4; Sigma, St. Louis, MO) injected by a 10 μ l syringe held by a microinjector (Insight, Ribeirão Preto, Brazil) and connected to 27 gauge injecting needles by polyethylene tubes. In the dHPC, 0.45 μ l of NMDA was injected at a rate of 15 μ l/min in each of the following coordinates: (1) AP: - 2.8 mm, ML: ± 1.5 mm and DV: - 3.6 mm; (2) AP: - 4.2 mm, ML: ± 1.5 and ± 4.0 mm and DV: - 4.0 mm. In the Per, 0.1 μ l of NMDA was injected (0.1 μ l/min) in each of the following coordinates: AP: - 2.6, - 3.5, - 4.4, - 5.4 and - 6.5 mm, ML: ± 5.9 , ± 6.1 , ± 6.1 , ± 6.5 and ± 6.4 mm, DV: - 7.4, - 7.4, - 7.4, - 7.2 and - 7.0. The needle remained in place for an additional 3 min. The post-surgical procedures were identical to those in Experiment 1.

In Experiment 3, surgeries were performed as in Experiment 2, but for lesions of the dHPC, disgranular retrosplenial (RSC), both (dHPC-RSC) or SHAMs. In the RSC, 0.2 μ l of 20 mg/ml NMDA was injected (0.1 μ l/min) in the following coordinates: AP: - 3.0, -4.0, - 5.0, - 6.0 and - 7.3 mm, ML: ± 0.4 , ± 0.4 , ± 0.5 , ± 0.7 and ± 0.8 mm, DV: - 0.8, - 1.0, - 1.0, - 1.1 and - 1.5 mm.

Apparatus

We used a fear conditioning chamber (32 x 25 x 25 cm, Med Associates, St. Albans, VT) equipped with Video Freeze System. The chamber was composed of aluminum (sidewalls), polycarbonate (front wall and ceiling), white opaque acrylic (back) pieces and a grid floor of stainless steel rods (4.8 mm thick) spaced 1.6 cm apart. A sound-attenuating chamber with fans (60 dB) provided background noise and white house lights enclosed the chamber. After each animal, the chamber was cleaned with 10% ethanol.

Contextual fear conditioning (CFC)

Before every experiment, all animals were gently handled for 3 consecutive days.

In Experiment 1, during the training session, the rats were individually placed into the conditioning chamber for 2 min, received a 1 s, 0.8 mA footshock, and were returned to their homecage after 1 min. One additional control group of SHAM animals (Imm) was placed in the conditioning chamber, received an immediate footshock and was immediately returned to the homecage. Half of the cohort was re-exposed to the context 48h later for 5 min to test contextual fear memory. Behavior was recorded in both sessions by a micro-camera in the chamber. An experimenter blind to the grouping measured the freezing behavior, defined as complete immobility except for breathing movements [94], which served as our measure of contextual fear memory.

In Experiments 2 and 3, rats were placed into the conditioning chamber for 2 min, but received three 1 s, 0.8 mA footshocks, with 30 s inter-trial interval, and were returned to their homecage after 1 min. The rest of the procedure is identical to Experiment 1, except that there was no Imm control group.

Perfusion and immunohistochemistry

Phosphorylated CREB (pCREB) has a two-phase peak expression profile, which the latter (3–6 h) was shown to present a clearer associative learning-specific expression [95, 96]. Therefore, we used a 3h time window of pCREB expression in our study. Three hours following training in Experiment 1, half the cohort was deeply anesthetized and perfused transcardially with buffered saline and 4% parahormaldehyde (PFA) in 0.1 M sodium buffer (pH 7.4). The brains were extracted, post-fixed in PFA, cryoprotected in 20% buffered sucrose, frozen and stored at -80°C. The brains were coronally sectioned in 30 μm thick slices in a cryostat (Leica, Wetzlar, Germany) and stored in 4 serial sets. One set was collected in glass slides and stained with cresyl violet for morphological and lesion analysis, another set was used for phospho-CREB immunolabelling and the two remaining were stored for future studies.

Immunolabelling was performed in free-floating sections using anti-phospho-CREB (1:1000, Santa Cruz, Dallas, TX) as primary rabbit polyclonal antibody. A Biotinylated goat anti-rabbit antibody (1:800, Vector Labs, Burlingame, CA) was used as secondary antibody. The reaction was revealed using the avidin-biotin peroxidase method conjugated to diaminobenzidine as the chromogen (ABC and DAB kits, Vector Labs, Burlingame, CA) as described previously [97].

pCREB quantification

The pCREB expression was measured in 30 brain regions including hippocampal, parahippocampal, amygdalar and prefrontal regions (see Fig 2) previously shown to have involvement in FC and/or context learning. The dHPC group had 27 regions measured, since dCA1, dCA3 and dDG were damaged. The regions were delimited manually using ImageJ free software. The anatomical delimitation was based on the Rat Brain Atlas Paxinos and Watson [98] as on other anatomical studies [see Fig 2; 99, 100, 101]. Images (32-bit RGB) were taken at 4X and 10X magnifications using a light microscope (Olympus, Waltham, MA), and pCREB-positive cells quantified using the automated, high-throughput, open-source CellProfiler software [102]. A pipeline was created to calculate the area of each region in mm² and to identify stained nuclei based on their intensity, shape and size (20–150 μm²; Fig 2B and 2C). The quantification was performed bilaterally in 6 sections/region (3 in each hemisphere). The data was expressed in nuclei density (nuclei/mm²). In each region and animal, three sections quantified bilaterally were averaged and computed as the expression data.

The pCREB is known to possess both a higher baseline and a higher expression profile (around twofold) compared to *c-fos*, an IEG more commonly used as a proxy for neuronal activity [95, 103, 104]. Although a baseline signal close to zero is preferable in most studies, for correlation-based connectivity inference it blunts sensitivity to observe negative correlations, as a diminished expression is less observable. Detecting possible negative correlations was desired in our study, making pCREB a suitable proxy for neuronal activity. Further, pCREB has a well distinguishable expression in associative learning studies [95, 96, 103].

Histology

In all experiments, the histological examination of the lesions was performed in the cresyl violet stained slices (150 μm apart) using a light microscope (Olympus, Waltham, MA). Lesions were identified visually as presence of tissue necrosis, absence of tissue or marked tissue thinning. Animals with no bilateral lesions of the target region or with lesions present in less than half the slices analyzed were excluded. An expressive bilateral lesion (50%) of untargeted regions was also an exclusionary criterion.

We photographed the histological sections at 4X magnification from bregma -2.10 mm to -7.10 mm (150 μ m apart). Next, we quantified the percentage of damaged tissue in the dHPC, RSC and dHPC_RSC groups. Using the NIH/ImageJ open source program, we quantified the area of spared tissue in each region and then calculated their overall volume. We quantified the intact RSC and RSGd in the dHPC group and the intact dHPC in the RSC group, then calculated the mean total volume of each of these regions and used these measures as the total intact volume for each region. For each region and subject, we calculated the percentage of spared tissue by dividing the spared volume by the total intact volume, then estimated the percentage of damaged tissue [1—spared volume].

Functional connectivity and network generation

Different from the typical neuroimaging studies in humans, which acquire multiple measurements across time (i.e. EEG, fMRI), task-dependent large-scale brain activity in experimental animals is more limited. As immunohistochemistry provides a single *post-mortem* measure per region per animal, inter-regional co-activation is assessed across subjects. We used the pCREB-positive nuclei density to compute the Pearson correlation coefficient between all possible pairs of regions in each group (total of 435 coefficients in SHAM and 351 in the dHPC group). As SHAM matrix has 3 regions (dCA1, dCA3 and dDG) more than dHPC matrix, a “SHAM with no dorsal hippocampal regions” (SHAM-nH) was also calculated. The network derived from this matrix served to directly compare the network of these groups. Three thresholds were applied to the correlation matrices, maintaining only coefficients with (uncorrected) two-tailed significance level of $p \leq 0.05$, 0.025 or 0.01. This resulted in weighted undirected network graphs composed by the brain regions (nodes) and the remaining inter-regional correlations (edges), representing connections between the regions (Fig 3). The network analyses were performed in the networks of all thresholds.

Network measures

Topological metrics. This analysis was performed in distance (1—Pearson’s r) matrices derived from the thresholded correlation matrices. We assessed the networks topology using global efficiency (Geff) as our measure of integration and mean local efficiency (Leff) as our measure of segregation [32]. Geff is defined as the mean of the inverse of all shortest paths in the network. And Leff is defined as the Geff applied to a subgraph composed by all neighbors of a given node.

Brain networks have been consistently characterized as possessing a small-world topology [21, 38, 105]. Small-worldness is usually estimated by metrics of integration and segregation, evincing equivalent integration and higher segregation relative to random networks [33]. We compared the Geff and mean Leff of our empirical networks to those of randomized networks to test whether the empirical networks were small-world. We also tested whether dHPC lesion affects the network small-worldness (i.e. Geff and mean Leff levels).

Centrality metrics and hub identification. Hubs were identified using four centrality metrics: weighted degree (Wdg), eigenvector (Evc), Closeness (Clo) and Betweenness (Bet). For each metric, we intersected the 25% most central regions (upper quartile) of all four metrics and considered any regions within the intersection of at least three metrics as a hub for that threshold. To ensure a hub identification that was irrespective of thresholding, we intersected the hubs in each threshold and considered a stable hub any region present in all thresholds. As Wdg and Evc are connection-based metrics (based on number of connections), and Clo and Bet are distance-based metrics (based on short paths), we ensured that these regions were highly ranked in at least one metric of each type.

Statistical analysis

In the cohort tested for fear memory, we compared the Total Freezing Time during memory test between the groups by three statistical tests: one-way ANOVA, Kolmogorov-Smirnov (KS) tests and Cohen's d effect size. In the ANOVAs and KS tests, we used a bootstrap resampling. The bootstrap resampling was defined by 1) randomly resampling the sample, with replacement of subjects by others (from the sample), 2) calculating the statistics of interest (i.e. $F_{\text{resampled}}$) and 3) repeating it many times (10000). It generates an empirical sample-based artificial distribution of the statistics of interest under the null hypothesis, and allows to test if the empirical data statistics ($F_{\text{empirical}}$) differs from random null hypothesis distribution. The p-value was calculated as the frequency of $F_{\text{empirical}}$ occurring in the resampled distribution [$p = (F_{\text{resampled}} > F_{\text{empirical}})/10000$]. There is no normality (or any other) assumption to bootstrap resampling tests, allowing comparisons when the population distribution is not normal or unknown. Multiple comparisons were assessed by t tests with bootstrap resampling, as above, correcting the p-value by the number of concomitant comparisons.

In the cohort that had their brains immunolabelled for pCREB, the pCREB expression was quantified in 30 regions (27 in the dHPC group) as positive nuclei/mm², and each region was compared between the groups using t tests with bootstrap resampling (as above), correcting the p-value with a false discovery rate (fdr) test [106].

In the hypothesis test for small-world network, each empirical network was 'rewired' as described previously [107] to generate 10000 random, null hypothesis networks with the same number of nodes, edges, weights and degree distribution. Each network was rewired a number of times equal to half the number of their edges to generate the randomized networks. We calculated the G_{eff} and mean L_{eff} empirical/random ratio for each randomized network. It was expected for the G_{eff} ratios to be around 1 and the mean L_{eff} ratios to be above 1. We also evaluated group differences in G_{eff} and mean L_{eff} ratios. Lack of overlap between any two 95% confidence interval was considered a significant difference.

After the hub identification, we directly compared the centrality level of each region (in each threshold) between the dHPC and SHAM-nH networks using a permutation test. In the permutation procedure, we 1) randomized the grouping labels without replacement, 2) calculated the centrality values differences [$\text{Diff} = C_{\text{SHAM}} - C_{\text{dHPC}}$] in each region and 3) repeated it 10000 times. The p-value was calculated as the frequency of the empirical difference ($\text{Diff}_{\text{empirical}}$) occurring in the resampled ($\text{Diff}_{\text{resampled}}$) distribution [$p = (\text{Diff}_{\text{resampled}} > \text{Diff}_{\text{empirical}})/10000$]. No comparisons with the SHAM network were performed as both networks have to be the same size.

To test whether dHPC lesion influences interactions between other regions in the network, we compared the correlation coefficients between SHAM-nH and dHPC networks. We normalized the thresholded matrices using a Fisher's Z transformation and compared the normalized correlation coefficient distributions in the dHPC and SHAM-nH networks with a two-sample KS test. Next, we calculated the z-score of the correlation coefficient difference between each cell of the matrices as in the formula below, defining an index of connectivity change, as done previously [74]. The Z-score values above |2| were considered significant (corresponding to a level of significance of $\alpha = 0.05$). We verified which group possessed each significantly higher coefficient, and which nodes they connect.

$$dC = \frac{R_{\text{sham}} - R_{\text{dHPC}}}{\sqrt{\frac{1}{(df_{\text{sham}} - 3)} + \frac{1}{(df_{\text{dHPC}} - 3)}}$$

where df is the degree of freedom in each group.

In all analyses, a corrected- $p < 0.05$ was considered significant. All statistical and graph theory analyses and figures were performed in R studio [108] using custom-written routines (available at https://github.com/coelhocao/Brain_Network_analysis) and the packages igraph [109], Matrix [110], lattice [111], ggplot2 [112], corrplot [113], car [114] and VennDiagram [115].

Supporting information

S1 Fig. Euclidian distance-based network configuration in each group. This network configuration reveals the regions that were more strongly correlated showing them closer to each other. The node sizes are proportional to the degree of each region. The edge width is proportional to its corresponding correlation coefficient. The networks are shown by group: SHAM (upper), SHAM-nH (middle) and dHPC (bottom); and by threshold: 0.05 (left), 0.025 (middle) and 0.01 (right). The node colors respect the code shown in Fig 2. (TIF)

S2 Fig. Hub identification in the SHAM network. The centrality values were ranked according to each metric (A) and each threshold. Non-grey regions indicate the upper 25% in each metric. Regions are colored according to the color code on Fig 2. The intersection of the upper 25% most central regions in each metric (B) showed the hubs in each threshold, defined as regions present in at least three of the four metrics (red contour). (TIF)

S3 Fig. Hub identification in the SHAM-nH network. The centrality values were ranked according to each metric (A) and each threshold. Non-grey regions indicate the upper 25% in each metric. Regions are colored according to the color code on Fig 2. The intersection of the upper 25% most central regions in each metric (B) showed the hubs in each threshold, defined as regions present in at least three of the four metrics (red contour). (TIF)

S4 Fig. Hub identification in the dHPC network. The centrality values were ranked according to each metric (A) and each threshold. Non-grey regions indicate the upper 25% in each metric. Regions are colored according to the color code on Fig 2. The intersection of the upper 25% most central regions in each metric (B) showed the hubs in each threshold, defined as regions present in at least three of the four metrics (red contour). (TIF)

S5 Fig. Detailed centrality comparison between SHAM-nH and dHPC networks. The comparison was done for each region, centrality metric and threshold. Values in each cell show the permutation test p -value for each comparison. Green round shades show significantly higher values in SHAM-nH, and blue round shades show significantly higher values in dHPC ($p < 0.05$). In each threshold, green lines indicate SHAM-nH network hubs for that threshold, and blue lines indicate dHPC network hubs. Values with lines and ground shades in the same color show hubs associated with significant differences. Wdg: Weighted Degree; Evc: Eigenvector; Clo: Closeness; Bet: Betweenness. This table is a detailed version of the Fig 7, where hub scores and differences can be seen by threshold. (TIF)

S6 Fig. Connectivity change in dHPC network by threshold. Cumulative distributions of the Fisher's Z transformed correlation coefficients from the SHAM-nH and dHPC matrices (Left). The “#” indicates that these distributions are significantly different (Kolmogorov-Smirnov test, $p < 0.05$). Cumulative distribution showing the z-score of the correlation coefficient differences

between the groups (Center). The dashed line shows the absolute Z-score of 2, revealing the values considered significant (beyond it) at the level of $\alpha = 0.05$. The significantly different coefficients were plotted in each network, showing the network and nodes to which it belonged (Right). Graphs shown for the networks in the 0.05 (A), 0.025 (B) and 0.01 (C) thresholds. (TIF)

S7 Fig. Impaired behavior in the dHPC_RSC group is independent of the incidental RSGd damage. (A) Mean and bootstrapped 95% IC of the percentage of damage in the RSC and RSGd in the RSC and dHPC_RSC groups and in the strict dHPC_RSC subgroup. Dots show the sample distribution in each group. (B) Mean and bootstrapped 95% IC of the total freezing time in the SHAM, dHPC, RSC, dHPC_RSC groups and the strict dHPC_RSC subgroup. Dots show the sample distribution in each group. (TIF)

S1 Text. Supporting experiments. We describe two supporting experiments in which we show, in a within-subject design, a task that is impaired by dHPC damage followed by an unimpaired performance at CFC. These tasks were the post-training CFC and the water maze. These experiments replicate classical findings on the effect of dHPC damage on spatial/contextual learning and memory. (DOCX)

S1 Data. Behavioral data acquired in Experiment 1. Organized by subject, group and total freezing time. (XLSX)

S2 Data. pCREB expression data acquired in Experiment 1. Organized by subject, group and brain region. (XLSX)

S3 Data. Behavioral data acquired in Experiment 2. Organized by subject, group and total freezing time. (XLSX)

S4 Data. Behavioral data acquired in Experiment 3. Organized by subject, group and total freezing time. (XLSX)

S5 Data. Behavioral data acquired in S Experiment 1. Organized by subject, group, test and total freezing time. (XLSX)

S6 Data. Behavioral data acquired in S Experiment 2. Organized by subject, group, day, phase, quadrant, latency and freezing time. (XLSX)

Acknowledgments

We thank André Fujita, André Cravo and Altay Lino de Souza for valuable comments and insights during the development of the study.

Author Contributions

Conceptualization: Cesar A. O. Coelho, Maria Gabriela M. Oliveira.

Data curation: Cesar A. O. Coelho.

Formal analysis: Cesar A. O. Coelho, Tatiana L. Ferreira, João R. Sato, Maria Gabriela M. Oliveira.

Funding acquisition: Cesar A. O. Coelho, Maria Gabriela M. Oliveira.

Investigation: Cesar A. O. Coelho, Juliana C. Kramer-Soares.

Methodology: Cesar A. O. Coelho, Tatiana L. Ferreira, Juliana C. Kramer-Soares, João R. Sato.

Project administration: Cesar A. O. Coelho, Maria Gabriela M. Oliveira.

Resources: Maria Gabriela M. Oliveira.

Software: Cesar A. O. Coelho, João R. Sato.

Supervision: João R. Sato, Maria Gabriela M. Oliveira.

Validation: Cesar A. O. Coelho.

Visualization: Cesar A. O. Coelho.

Writing – original draft: Cesar A. O. Coelho.

Writing – review & editing: Cesar A. O. Coelho, Tatiana L. Ferreira, Juliana C. Kramer-Soares, João R. Sato, Maria Gabriela M. Oliveira.

References

1. Geschwind N. Disconnexion syndromes in animals and man. I. Brain. 1965; 88(2):237–94. PMID: [5318481](#).
2. Aggleton JP. EPS Mid-Career Award 2006. Understanding anterograde amnesia: disconnections and hidden lesions. Q J Exp Psychol (Hove). 2008; 61(10):1441–71. <https://doi.org/10.1080/17470210802215335> PMID: [18671169](#).
3. Frankland PW, Cestari V, Filipkowski RK, McDonald RJ, Silva AJ. The dorsal hippocampus is essential for context discrimination but not for contextual conditioning. Behav Neurosci. 1998; 112(4):863–74. Epub 1998/09/11. PMID: [9733192](#).
4. Kjelstrup KG, Tuvnes FA, Steffenach HA, Murison R, Moser EI, Moser MB. Reduced fear expression after lesions of the ventral hippocampus. Proc Natl Acad Sci U S A. 2002; 99(16):10825–30. Epub 2002/08/01. <https://doi.org/10.1073/pnas.152112399> PMID: [12149439](#).
5. Richmond MA, Yee BK, Pouzet B, Veenman L, Rawlins JN, Feldon J, et al. Dissociating context and space within the hippocampus: effects of complete, dorsal, and ventral excitotoxic hippocampal lesions on conditioned freezing and spatial learning. Behav Neurosci. 1999; 113(6):1189–203. PMID: [10636298](#).
6. Wiltgen BJ, Sanders MJ, Anagnostaras SG, Sage JR, Fanselow MS. Context fear learning in the absence of the hippocampus. J Neurosci. 2006; 26(20):5484–91. Epub 2006/05/19. <https://doi.org/10.1523/JNEUROSCI.2685-05.2006> PMID: [16707800](#).
7. Gale GD, Anagnostaras SG, Fanselow MS. Cholinergic modulation of pavlovian fear conditioning: effects of intrahippocampal scopolamine infusion. Hippocampus. 2001; 11(4):371–6. Epub 2001/09/04. <https://doi.org/10.1002/hipo.1051> PMID: [11530841](#).
8. Schenberg EE, Oliveira MG. Effects of pre or posttraining dorsal hippocampus D-AP5 injection on fear conditioning to tone, background, and foreground context. Hippocampus. 2008; 18(11):1089–93. Epub 2008/08/30. <https://doi.org/10.1002/hipo.20475> PMID: [18727044](#).
9. Liu X, Ramirez S, Pang PT, Puryear CB, Govindarajan A, Deisseroth K, et al. Optogenetic stimulation of a hippocampal engram activates fear memory recall. Nature. 2012; 484(7394):381–5. Epub 2012/03/24. <https://doi.org/10.1038/nature11028> PMID: [22441246](#).
10. Nadel L, Willner J. Context and conditioning: a place for space. Physiological Psychology. 1980; 8(2):11.
11. Rudy JW. Context representations, context functions, and the parahippocampal-hippocampal system. Learn Mem. 2009; 16(10):573–85. Epub 2009/10/02. <https://doi.org/10.1101/lm.1494409> PMID: [19794181](#).

12. Fanselow MS. From contextual fear to a dynamic view of memory systems. *Trends Cogn Sci.* 2010; 14(1):7–15. Epub 2009/11/27. <https://doi.org/10.1016/j.tics.2009.10.008> PMID: 19939724.
13. Zelikowsky M, Bissiere S, Fanselow MS. Contextual fear memories formed in the absence of the dorsal hippocampus decay across time. *J Neurosci.* 2012; 32(10):3393–7. <https://doi.org/10.1523/JNEUROSCI.4339-11.2012> PMID: 22399761.
14. Nadel L. The Hippocampus and Context Revisited. In: Mizumori SJY, editor. *Hippocampal Place Fields: Relevance to Learning and Memory.* 1. New York: Oxford University Press; 2008. p. 3–15.
15. Fanselow MS, Poulos AM. The neuroscience of mammalian associative learning. *Annu Rev Psychol.* 2005; 56:207–34. Epub 2005/02/16. <https://doi.org/10.1146/annurev.psych.56.091103.070213> PMID: 15709934.
16. Maren S. Seeking a spotless mind: extinction, deconsolidation, and erasure of fear memory. *Neuron.* 2011; 70(5):830–45. Epub 2011/06/11. <https://doi.org/10.1016/j.neuron.2011.04.023> PMID: 21658578.
17. Bucci DJ, Robinson S. Toward a conceptualization of retrohippocampal contributions to learning and memory. *Neurobiol Learn Mem.* 2014; 116:197–207. <https://doi.org/10.1016/j.nlm.2014.05.007> PMID: 24878277.
18. Bullmore E, Sporns O. Complex brain networks: graph theoretical analysis of structural and functional systems. *Nat Rev Neurosci.* 2009; 10(3):186–98. Epub 2009/02/04. <https://doi.org/10.1038/nrn2575> PMID: 19190637.
19. Mišić B, Sporns O. From regions to connections and networks: new bridges between brain and behavior. *Curr Opin Neurobiol.* 2016; 40:1–7. Epub 2016/05/19. <https://doi.org/10.1016/j.conb.2016.05.003> PMID: 27209150.
20. Medaglia JD, Lynall ME, Bassett DS. Cognitive network neuroscience. *J Cogn Neurosci.* 2015; 27(8):1471–91. Epub 2015/03/24. https://doi.org/10.1162/jocn_a_00810 PMID: 25803596.
21. Achard S, Salvador R, Whitcher B, Suckling J, Bullmore E. A resilient, low-frequency, small-world human brain functional network with highly connected association cortical hubs. *J Neurosci.* 2006; 26(1):63–72. <https://doi.org/10.1523/JNEUROSCI.3874-05.2006> PMID: 16399673.
22. Bassett DS, Wymbs NF, Porter MA, Mucha PJ, Carlson JM, Grafton ST. Dynamic reconfiguration of human brain networks during learning. *Proc Natl Acad Sci U S A.* 2011; 108(18):7641–6. Epub 2011/04/18. <https://doi.org/10.1073/pnas.1018985108> PMID: 21502525.
23. Kinnison J, Padmala S, Choi JM, Pessoa L. Network analysis reveals increased integration during emotional and motivational processing. *J Neurosci.* 2012; 32(24):8361–72. <https://doi.org/10.1523/JNEUROSCI.0821-12.2012> PMID: 22699916.
24. van den Heuvel MP, Sporns O. Network hubs in the human brain. *Trends Cogn Sci.* 2013; 17(12):683–96. <https://doi.org/10.1016/j.tics.2013.09.012> PMID: 24231140.
25. Hillary FG, Grafman JH. Injured Brains and Adaptive Networks: The Benefits and Costs of Hyperconnectivity. *Trends Cogn Sci.* 2017. Epub 2017/03/31. <https://doi.org/10.1016/j.tics.2017.03.003> PMID: 28372878.
26. Sato JR, Balardin J, Vidal MC, Fujita A. Identification of segregated regions in the functional brain connectome of autistic patients by a combination of fuzzy spectral clustering and entropy analysis. *J Psychiatry Neurosci.* 2016; 41(2):124–32. <https://doi.org/10.1503/jpn.140364> PMID: 26505141.
27. Crossley NA, Fox PT, Bullmore ET. Meta-connectomics: human brain network and connectivity meta-analyses. *Psychol Med.* 2016; 46(5):897–907. Epub 2016/01/26. <https://doi.org/10.1017/S0033291715002895> PMID: 26809184.
28. Wheeler AL, Teixeira CM, Wang AH, Xiong X, Kovacevic N, Lerch JP, et al. Identification of a functional connectome for long-term fear memory in mice. *PLoS Comput Biol.* 2013; 9(1):e1002853. <https://doi.org/10.1371/journal.pcbi.1002853> PMID: 23300432.
29. Vetere G, Kenney JW, Tran LM, Xia F, Steadman PE, Parkinson J, et al. Chemogenetic Interrogation of a Brain-wide Fear Memory Network in Mice. *Neuron.* 2017; 94(2):363–74.e4. <https://doi.org/10.1016/j.neuron.2017.03.037> PMID: 28426969.
30. Alberini CM. Transcription factors in long-term memory and synaptic plasticity. *Physiol Rev.* 2009; 89(1):121–45. Epub 2009/01/08. <https://doi.org/10.1152/physrev.00017.2008> PMID: 19126756.
31. Zelikowsky M, Bissiere S, Hast TA, Bennett RZ, Abdipranoto A, Vissel B, et al. Prefrontal microcircuit underlies contextual learning after hippocampal loss. *Proc Natl Acad Sci U S A.* 2013; 110(24):9938–43. Epub 2013/05/15. <https://doi.org/10.1073/pnas.1301691110> PMID: 23676273.
32. Latora V, Marchiori M. Efficient behavior of small-world networks. *Phys Rev Lett.* 2001; 87(19):198701. <https://doi.org/10.1103/PhysRevLett.87.198701> PMID: 11690461.
33. Watts DJ, Strogatz SH. Collective dynamics of 'small-world' networks. *Nature.* 1998; 393(6684):440–2. <https://doi.org/10.1038/30918> PMID: 9623998.

34. Phillips RG, LeDoux JE. Lesions of the fornix but not the entorhinal or perirhinal cortex interfere with contextual fear conditioning. *J Neurosci*. 1995; 15(7 Pt 2):5308–15. Epub 1995/07/01. PMID: [7623153](https://pubmed.ncbi.nlm.nih.gov/7623153/).
35. Herzog C, Otto T. Contributions of anterior perirhinal cortex to olfactory and contextual fear conditioning. *Neuroreport*. 1998; 9(8):1855–9. PMID: [9665615](https://pubmed.ncbi.nlm.nih.gov/9665615/).
36. Bucci DJ, Phillips RG, Burwell RD. Contributions of postrhinal and perirhinal cortex to contextual information processing. *Behav Neurosci*. 2000; 114(5):882–94. Epub 2000/11/21. PMID: [11085602](https://pubmed.ncbi.nlm.nih.gov/11085602/).
37. Bassett DS, Bullmore E. Small-world brain networks. *Neuroscientist*. 2006; 12(6):512–23. <https://doi.org/10.1177/1073858406293182> PMID: [17079517](https://pubmed.ncbi.nlm.nih.gov/17079517/).
38. Bassett DS, Bullmore ET. Small-World Brain Networks Revisited. *Neuroscientist*. 2016. Epub 2016/09/21. <https://doi.org/10.1177/1073858416667720> PMID: [27655008](https://pubmed.ncbi.nlm.nih.gov/27655008/).
39. Achard S, Bullmore E. Efficiency and cost of economical brain functional networks. *PLoS Comput Biol*. 2007; 3(2):e17. <https://doi.org/10.1371/journal.pcbi.0030017> PMID: [17274684](https://pubmed.ncbi.nlm.nih.gov/17274684/).
40. Hermundstad AM, Brown KS, Bassett DS, Carlson JM. Learning, memory, and the role of neural network architecture. *PLoS Comput Biol*. 2011; 7(6):e1002063. Epub 2011/06/30. <https://doi.org/10.1371/journal.pcbi.1002063> PMID: [21738455](https://pubmed.ncbi.nlm.nih.gov/21738455/).
41. Zippo AG, Storchi R, Nencini S, Caramenti GC, Valente M, Biella GE. Neuronal functional connection graphs among multiple areas of the rat somatosensory system during spontaneous and evoked activities. *PLoS Comput Biol*. 2013; 9(6):e1003104. Epub 2013/06/13. <https://doi.org/10.1371/journal.pcbi.1003104> PMID: [23785273](https://pubmed.ncbi.nlm.nih.gov/23785273/).
42. Bassett DS, Meyer-Lindenberg A, Achard S, Duke T, Bullmore E. Adaptive reconfiguration of fractal small-world human brain functional networks. *Proc Natl Acad Sci U S A*. 2006; 103(51):19518–23. Epub 2006/12/11. <https://doi.org/10.1073/pnas.0606005103> PMID: [17159150](https://pubmed.ncbi.nlm.nih.gov/17159150/).
43. Kitzbichler MG, Henson RN, Smith ML, Nathan PJ, Bullmore ET. Cognitive effort drives workspace configuration of human brain functional networks. *J Neurosci*. 2011; 31(22):8259–70. <https://doi.org/10.1523/JNEUROSCI.0440-11.2011> PMID: [21632947](https://pubmed.ncbi.nlm.nih.gov/21632947/).
44. Ekman M, Derrfuss J, Tittgemeyer M, Fiebach CJ. Predicting errors from reconfiguration patterns in human brain networks. *Proc Natl Acad Sci U S A*. 2012; 109(41):16714–9. Epub 2012/09/24. <https://doi.org/10.1073/pnas.1207523109> PMID: [23012417](https://pubmed.ncbi.nlm.nih.gov/23012417/).
45. Fornito A, Harrison BJ, Zalesky A, Simons JS. Competitive and cooperative dynamics of large-scale brain functional networks supporting recollection. *Proc Natl Acad Sci U S A*. 2012; 109(31):12788–93. Epub 2012/07/17. <https://doi.org/10.1073/pnas.1204185109> PMID: [22807481](https://pubmed.ncbi.nlm.nih.gov/22807481/).
46. Ritchey M, Libby LA, Ranganath C. Cortico-hippocampal systems involved in memory and cognition: the PMAT framework. *Prog Brain Res*. 2015; 219:45–64. Epub 2015/05/23. <https://doi.org/10.1016/bs.pbr.2015.04.001> PMID: [26072233](https://pubmed.ncbi.nlm.nih.gov/26072233/).
47. Suzuki WA, Naya Y. The perirhinal cortex. *Annu Rev Neurosci*. 2014; 37:39–53. <https://doi.org/10.1146/annurev-neuro-071013-014207> PMID: [25032492](https://pubmed.ncbi.nlm.nih.gov/25032492/).
48. Kealy J, Commins S. The rat perirhinal cortex: A review of anatomy, physiology, plasticity, and function. *Prog Neurobiol*. 2011; 93(4):522–48. <https://doi.org/10.1016/j.pneurobio.2011.03.002> PMID: [21420466](https://pubmed.ncbi.nlm.nih.gov/21420466/).
49. Kinnavane L, Amin E, Olarte-Sánchez CM, Aggleton JP. Medial temporal pathways for contextual learning: Network c-fos mapping in rats with or without perirhinal cortex lesions. *Brain Neurosci Adv*. 2017; 1. <https://doi.org/10.1177/2398212817694167> PMID: [28685167](https://pubmed.ncbi.nlm.nih.gov/28685167/).
50. Todd TP, Bucci DJ. Retrosplenial Cortex and Long-Term Memory: Molecules to Behavior. *Neural Plast*. 2015; 2015:414173. Epub 2015/08/25. <https://doi.org/10.1155/2015/414173> PMID: [26380115](https://pubmed.ncbi.nlm.nih.gov/26380115/).
51. Vann SD, Aggleton JP, Maguire EA. What does the retrosplenial cortex do? *Nat Rev Neurosci*. 2009; 10(11):792–802. <https://doi.org/10.1038/nrn2733> PMID: [19812579](https://pubmed.ncbi.nlm.nih.gov/19812579/).
52. Auger SD, Mullally SL, Maguire EA. Retrosplenial cortex codes for permanent landmarks. *PLoS One*. 2012; 7(8):e43620. Epub 2012/08/17. <https://doi.org/10.1371/journal.pone.0043620> PMID: [22912894](https://pubmed.ncbi.nlm.nih.gov/22912894/).
53. Auger SD, Zeidman P, Maguire EA. A central role for the retrosplenial cortex in de novo environmental learning. *Elife*. 2015; 4. Epub 2015/08/18. <https://doi.org/10.7554/eLife.09031> PMID: [26284602](https://pubmed.ncbi.nlm.nih.gov/26284602/).
54. Auger SD, Zeidman P, Maguire EA. Efficacy of navigation may be influenced by retrosplenial cortex-mediated learning of landmark stability. *Neuropsychologia*. 2017; 104:102–12. Epub 2017/08/10. <https://doi.org/10.1016/j.neuropsychologia.2017.08.012> PMID: [28802770](https://pubmed.ncbi.nlm.nih.gov/28802770/).
55. Alexander AS, Nitz DA. Retrosplenial cortex maps the conjunction of internal and external spaces. *Nat Neurosci*. 2015; 18(8):1143–51. <https://doi.org/10.1038/nn.4058> PMID: [26147532](https://pubmed.ncbi.nlm.nih.gov/26147532/).

56. Jacob PY, Casali G, Spieser L, Page H, Overington D, Jeffery K. An independent, landmark-dominated head-direction signal in dysgranular retrosplenial cortex. *Nat Neurosci.* 2017; 20(2):173–5. Epub 2016/12/19. <https://doi.org/10.1038/nn.4465> PMID: 27991898.
57. Czajkowski R, Jayaprakash B, Wiltgen B, Rogerson T, Guzman-Karlsson MC, Barth AL, et al. Encoding and storage of spatial information in the retrosplenial cortex. *Proc Natl Acad Sci U S A.* 2014; 111(23):8661–6. Epub 2014/05/27. <https://doi.org/10.1073/pnas.1313222111> PMID: 24912150.
58. Pothuizen HH, Aggleton JP, Vann SD. Do rats with retrosplenial cortex lesions lack direction? *Eur J Neurosci.* 2008; 28(12):2486–98. <https://doi.org/10.1111/j.1460-9568.2008.06550.x> PMID: 19032585.
59. Nelson AJ, Powell AL, Holmes JD, Vann SD, Aggleton JP. What does spatial alternation tell us about retrosplenial cortex function? *Front Behav Neurosci.* 2015; 9:126. <https://doi.org/10.3389/fnbeh.2015.00126> PMID: 26042009.
60. Keene CS, Bucci DJ. Neurotoxic lesions of retrosplenial cortex disrupt signaled and unsignaled contextual fear conditioning. *Behav Neurosci.* 2008; 122(5):1070–7. <https://doi.org/10.1037/a0012895> PMID: 18823164.
61. Todd TP, DeAngeli NE, Jiang MY, Bucci DJ. Retrograde amnesia of contextual fear conditioning: Evidence for retrosplenial cortex involvement in configural processing. *Behav Neurosci.* 2017; 131(1):46–54. Epub 2017/01/05. <https://doi.org/10.1037/bne0000183> PMID: 28054807.
62. Cowansage KK, Shuman T, Dillingham BC, Chang A, Golshani P, Mayford M. Direct reactivation of a coherent neocortical memory of context. *Neuron.* 2014; 84(2):432–41. Epub 2014/10/09. <https://doi.org/10.1016/j.neuron.2014.09.022> PMID: 25308330.
63. Cooper BG, Mizumori SJ. Temporary inactivation of the retrosplenial cortex causes a transient reorganization of spatial coding in the hippocampus. *J Neurosci.* 2001; 21(11):3986–4001. PMID: 11356886.
64. Robinson S, Poorman CE, Marder TJ, Bucci DJ. Identification of functional circuitry between retrosplenial and postrhinal cortices during fear conditioning. *J Neurosci.* 2012; 32(35):12076–86. <https://doi.org/10.1523/JNEUROSCI.2814-12.2012> PMID: 22933791.
65. Hillary FG, Roman CA, Venkatesan U, Rajtmajer SM, Bajo R, Castellanos ND. Hyperconnectivity is a fundamental response to neurological disruption. *Neuropsychology.* 2015; 29(1):59–75. Epub 2014/06/16. <https://doi.org/10.1037/neu0000110> PMID: 24933491.
66. Hillary FG, Rajtmajer SM, Roman CA, Medaglia JD, Slocomb-Dluzen JE, Calhoun VD, et al. The rich get richer: brain injury elicits hyperconnectivity in core subnetworks. *PLoS One.* 2014; 9(8):e104021. Epub 2014/08/14. <https://doi.org/10.1371/journal.pone.0104021> PMID: 25121760.
67. Turner GR, Levine B. Augmented neural activity during executive control processing following diffuse axonal injury. *Neurology.* 2008; 71(11):812–8. <https://doi.org/10.1212/01.wnl.0000325640.18235.1c> PMID: 18779509.
68. Turner GR, McIntosh AR, Levine B. Prefrontal Compensatory Engagement in TBI is due to Altered Functional Engagement Of Existing Networks and not Functional Reorganization. *Front Syst Neurosci.* 2011; 5:9. Epub 2011/02/24. <https://doi.org/10.3389/fnsys.2011.00009> PMID: 21412403.
69. Grady CL, McIntosh AR, Beig S, Keightley ML, Burian H, Black SE. Evidence from functional neuroimaging of a compensatory prefrontal network in Alzheimer's disease. *J Neurosci.* 2003; 23(3):986–93. PMID: 12574428.
70. Medaglia JD, Chiou KS, Slocomb J, Fitzpatrick NM, Wardecker BM, Ramanathan D, et al. The less BOLD, the wiser: support for the latent resource hypothesis after traumatic brain injury. *Hum Brain Mapp.* 2012; 33(4):979–93. Epub 2011/05/17. <https://doi.org/10.1002/hbm.21264> PMID: 21591026.
71. Hillary FG, Genova HM, Medaglia JD, Fitzpatrick NM, Chiou KS, Wardecker BM, et al. The nature of processing speed deficits in traumatic brain injury: is less brain more? *Brain Imaging Behav.* 2010; 4(2):141–54. <https://doi.org/10.1007/s11682-010-9094-z> PMID: 20502993.
72. Hillary FG. Neuroimaging of working memory dysfunction and the dilemma with brain reorganization hypotheses. *J Int Neuropsychol Soc.* 2008; 14(4):526–34. <https://doi.org/10.1017/S1355617708080788> PMID: 18577281.
73. Caeyenberghs K, Verhelst H, Clemente A, Wilson PH. Mapping the functional connectome in traumatic brain injury: What can graph metrics tell us? *Neuroimage.* 2016. Epub 2016/12/03. <https://doi.org/10.1016/j.neuroimage.2016.12.003> PMID: 27919750.
74. Alstott J, Breakspear M, Hagmann P, Cammoun L, Sporns O. Modeling the impact of lesions in the human brain. *PLoS Comput Biol.* 2009; 5(6):e1000408. <https://doi.org/10.1371/journal.pcbi.1000408> PMID: 19521503.
75. Corbetta M, Kincade MJ, Lewis C, Snyder AZ, Sapir A. Neural basis and recovery of spatial attention deficits in spatial neglect. *Nature Neuroscience.* 2005; 8:1603–10. <https://doi.org/10.1038/nn1574> PMID: 16234807.

76. He BJ, Snyder AZ, Vincent JL, Epstein A, Shulman GL, Corbetta M. Breakdown of Functional Connectivity in Frontoparietal Networks Underlies Behavioral Deficits in Spatial Neglect. *Neuron*. 2007; 53(6):905–18 <https://doi.org/10.1016/j.neuron.2007.02.013> PMID: 17359924
77. Burwell RD, Bucci DJ, Sanborn MR, Jutras MJ. Perirhinal and postrhinal contributions to remote memory for context. *J Neurosci*. 2004; 24(49):11023–8. Epub 2004/12/14. <https://doi.org/10.1523/JNEUROSCI.3781-04.2004> PMID: 15590918.
78. Albrechet-Souza L, Borelli KG, Almada RC, Brandão ML. Midazolam reduces the selective activation of the rhinal cortex by contextual fear stimuli. *Behav Brain Res*. 2011; 216(2):631–8. Epub 2010/09/19. <https://doi.org/10.1016/j.bbr.2010.09.006> PMID: 20851717.
79. Corcoran KA, Donnan MD, Tronson NC, Guzmán YF, Gao C, Jovasevic V, et al. NMDA receptors in retrosplenial cortex are necessary for retrieval of recent and remote context fear memory. *J Neurosci*. 2011; 31(32):11655–9. <https://doi.org/10.1523/JNEUROSCI.2107-11.2011> PMID: 21832195.
80. Keene CS, Bucci DJ. Contributions of the retrosplenial and posterior parietal cortices to cue-specific and contextual fear conditioning. *Behav Neurosci*. 2008; 122(1):89–97. <https://doi.org/10.1037/0735-7044.122.1.89> PMID: 18298252.
81. Lukoyanov NV, Lukoyanova EA. Retrosplenial cortex lesions impair acquisition of active avoidance while sparing fear-based emotional memory. *Behav Brain Res*. 2006; 173(2):229–36. Epub 2006/07/31. <https://doi.org/10.1016/j.bbr.2006.06.026> PMID: 16876887.
82. Eacott MJ, Machin PE, Gaffan EA. Elemental and configural visual discrimination learning following lesions to perirhinal cortex in the rat. *Behav Brain Res*. 2001; 124(1):55–70. PMID: 11423166.
83. Hales JB, Broadbent NJ, Velu PD, Squire LR, Clark RE. Hippocampus, perirhinal cortex, and complex visual discriminations in rats and humans. *Learn Mem*. 2015; 22(2):83–91. <https://doi.org/10.1101/lm.035840.114> PMID: 25593294.
84. Nelson AJ, Hindley EL, Pearce JM, Vann SD, Aggleton JP. The effect of retrosplenial cortex lesions in rats on incidental and active spatial learning. *Front Behav Neurosci*. 2015; 9:11. <https://doi.org/10.3389/fnbeh.2015.00011> PMID: 25705182.
85. Hindley EL, Nelson AJ, Aggleton JP, Vann SD. The rat retrosplenial cortex is required when visual cues are used flexibly to determine location. *Behav Brain Res*. 2014; 263:98–107. <https://doi.org/10.1016/j.bbr.2014.01.028> PMID: 24486256.
86. Winocur G, Moscovitch M, Rosenbaum RS, Sekeres M. An investigation of the effects of hippocampal lesions in rats on pre- and postoperatively acquired spatial memory in a complex environment. *Hippocampus*. 2010; 20(12):1350–65. <https://doi.org/10.1002/hipo.20721> PMID: 20054817.
87. Roy DS, Kitamura T, Okuyama T, Ogawa SK, Sun C, Obata Y, et al. Distinct Neural Circuits for the Formation and Retrieval of Episodic Memories. *Cell*. 2017; 170(5):1000–12.e19. Epub 2017/08/17. <https://doi.org/10.1016/j.cell.2017.07.013> PMID: 28823555.
88. Tonegawa S, Pignatelli M, Roy DS, Ryan TJ. Memory engram storage and retrieval. *Curr Opin Neurobiol*. 2015; 35:101–9. Epub 2015/08/14. <https://doi.org/10.1016/j.conb.2015.07.009> PMID: 26280931.
89. Squire LR, Genzel L, Wixted JT, Morris RG. Memory consolidation. *Cold Spring Harb Perspect Biol*. 2015; 7(8):a021766. Epub 2015/08/03. <https://doi.org/10.1101/cshperspect.a021766> PMID: 26238360.
90. van Wijk BC, Stam CJ, Daffertshofer A. Comparing brain networks of different size and connectivity density using graph theory. *PLoS One*. 2010; 5(10):e13701. Epub 2010/10/28. <https://doi.org/10.1371/journal.pone.0013701> PMID: 21060892.
91. Bota M, Sporns O, Swanson LW. Architecture of the cerebral cortical association connectome underlying cognition. *Proc Natl Acad Sci U S A*. 2015; 112(16):E2093–101. <https://doi.org/10.1073/pnas.1504394112> PMID: 25848037.
92. Biniewicz FZ, van Strien NM, Wadman WJ, van den Heuvel MP, Cappaert NL. Graph analysis of the anatomical network organization of the hippocampal formation and parahippocampal region in the rat. *Brain Struct Funct*. 2015. <https://doi.org/10.1007/s00429-015-0992-0> PMID: 25618022.
93. Petersen SE, Sporns O. Brain Networks and Cognitive Architectures. *Neuron*. 2015; 88(1):207–19. <https://doi.org/10.1016/j.neuron.2015.09.027> PMID: 26447582.
94. Bouton ME, Bolles RC. Conditioned fear assessed by freezing and by the suppression of three different baselines. *Anita Learn Behav*. 1980; 8:6.
95. Stanciu M, Radulovic J, Spiess J. Phosphorylated cAMP response element binding protein in the mouse brain after fear conditioning: relationship to Fos production. *Brain Res Mol Brain Res*. 2001; 94(1–2):15–24. Epub 2001/10/13. PMID: 11597761.
96. Trifilieff P, Herry C, Vanhoutte P, Caboche J, Desmedt A, Riedel G, et al. Foreground contextual fear memory consolidation requires two independent phases of hippocampal ERK/CREB activation. *Learn Mem*. 2006; 13(3):349–58. Epub 2006/05/18. <https://doi.org/10.1101/lm.80206> PMID: 16705140.

97. de Oliveira Coelho CA, Ferreira TL, Soares JC, Oliveira MG. Hippocampal NMDA receptor blockade impairs CREB phosphorylation in amygdala after contextual fear conditioning. *Hippocampus*. 2013. Epub 2013/03/06. <https://doi.org/10.1002/hipo.22118> PMID: 23460450.
98. Paxinos G, Watson C. *The Rat Brain in stereotaxic coordinates*. London, UK: Academic Press; 2007.
99. Burwell RD. Borders and cytoarchitecture of the perirhinal and postrhinal cortices in the rat. *J Comp Neurol*. 2001; 437(1):17–41. PMID: 11477594.
100. Insausti R, Herrero MT, Witter MP. Entorhinal cortex of the rat: cytoarchitectonic subdivisions and the origin and distribution of cortical efferents. *Hippocampus*. 1997; 7(2):146–83. PMID: 9136047.
101. Sugar J, Witter MP, van Strien NM, Cappaert NL. The retrosplenial cortex: intrinsic connectivity and connections with the (para)hippocampal region in the rat. An interactive connectome. *Front Neuroinform*. 2011; 5:7. <https://doi.org/10.3389/fninf.2011.00007> PMID: 21847380.
102. Carpenter AE, Jones TR, Lamprecht MR, Clarke C, Kang IH, Friman O, et al. CellProfiler: image analysis software for identifying and quantifying cell phenotypes. *Genome Biol*. 2006; 7(10):R100. <https://doi.org/10.1186/gb-2006-7-10-r100> PMID: 17076895.
103. Colombo PJ, Brightwell JJ, Countryman RA. Cognitive strategy-specific increases in phosphorylated cAMP response element-binding protein and c-Fos in the hippocampus and dorsal striatum. *J Neurosci*. 2003; 23(8):3547–54. PMID: 12716964.
104. Hall J, Thomas KL, Everitt BJ. Fear memory retrieval induces CREB phosphorylation and Fos expression within the amygdala. *Eur J Neurosci*. 2001; 13(7):1453–8. Epub 2001/04/12. PMID: 11298807.
105. Sporns O, Zwi JD. The small world of the cerebral cortex. *Neuroinformatics*. 2004; 2(2):145–62. <https://doi.org/10.1385/Nl:2:2:145> PMID: 15319512.
106. Benjamini Y, Hochberg Y. Controlling the False Discovery Rate: A Practical and Powerful Approach to Multiple Testing. *Journal of the Royal Statistical Society Series B (Methodological)*. 1995; 57(1):289–300.
107. Maslov S, Sneppen K. Specificity and stability in topology of protein networks. *Science*. 2002; 296(5569):910–3. <https://doi.org/10.1126/science.1065103> PMID: 11988575.
108. R CT. *R: A Language and Environment for Statistical Computing*. Vienna, Austria: R Foundation for Statistical Computing; 2013.
109. Csardi G, Nepusz T. The igraph software package for complex network research. *InterJournal*; 2006. p. 1695.
110. Bates D, Maechler M. *Matrix: Sparse and Dense Matrix Classes and Methods*. R package version 1.2–3 ed2015. p. <http://CRAN.R-project.org/package=Matrix>
111. Sakar D. *Lattice: Multivariate Data Visualization with R*. New York: Springer; 2008.
112. Wickham H. *ggplot2: Elegant Graphics for Data Analysis*. Springer-Verlag New York; 2009.
113. Wei Tn. *corrplot: Visualization of a correlation matrix*. 2013.
114. Fox J, Weisberg S. *An R Companion to Applied Regression*. second ed. Thousand Oaks, CA: Sage; 2011.
115. Chen H. *VennDiagram: Generate High-Resolution Venn and Euler Plots*. 2015.